Energy dependence of the charged multiplicity in deep inelastic scattering at HERA

The ZEUS collaboration

ABSTRACT: The charged multiplicity distributions and the mean charged multiplicity have been investigated in inclusive neutral current deep inelastic ep scattering with the ZEUS detector at HERA, using an integrated luminosity of 38.6 pb^{-1}. The measurements were performed in the current region of the Breit frame, as well as in the current fragmentation region of the hadronic centre-of-mass frame. The KNO-scaling properties of the data were investigated and the energy dependence was studied using different energy scales. The data are compared to results obtained in e^+e^- collisions and to previous DIS measurements as well as to leading-logarithm parton-shower Monte Carlo predictions.

Contents

1. Introduction

The production of multi-hadronic final states in high-energy two-body collisions has long been a subject of great interest from experimental and theoretical points of view. The charged multiplicity at HERA has been measured previously by the H1 [1 – 4] and ZEUS [5 – 7] experiments. In this paper, new measurements by the ZEUS collaboration of the charged multiplicity in deep inelastic scattering (DIS) are presented.

Measurements are performed in the hadronic centre-of-mass (HCM) frame and the results are compared with those obtained in e^+e^- collisions, as well as with those from previous DIS experiments [1, 8 – 10]. For the ep final state, differences are expected in the photon (current) and proton (target) fragmentation regions, due to the asymmetric nature of the reaction. The detector acceptance only allows the current fragmentation region to be measured.

Measurements of the charged multiplicity are also performed in the current region of the Breit frame, which should behave similarly to one hemisphere in e^+e^- collisions. Previous DIS results [2, 5, 11] using Q, the virtuality of the exchanged photon, as the scale showed a reasonable agreement with e^+e^- data. However, this agreement degraded

at values of Q below 6–8 GeV. In this paper, the energy of the current region of the Breit frame is used as the scale to compare with e^+e^- data.

An alternative energy scale, the invariant mass of the hadronic system, has also been used in both the Breit and HCM frames. The results using this variable are also compared to results from e^+e^- collisions.

2. Experimental set-up

The data were collected with the ZEUS detector during the 1996 and 1997 running periods, when HERA operated with protons of energy $E_p = 820$ GeV and positrons of energy $E_e = 27.5$ GeV, and correspond to an integrated luminosity of 38.6 ± 0.6 pb^{-1}.

The ZEUS detector is described in detail elsewhere [12]. The most important components used in the current analysis were the central tracking detector and the calorimeter.

Charged particles were tracked in the central tracking detector (CTD) [13–15], which operated in a magnetic field of 1.43 T provided by a thin superconducting coil. The CTD consisted of 72 cylindrical drift chamber layers, organised in 9 superlayers covering the polar-angle[1] region $15° < \theta < 164°$. The transverse-momentum resolution for full-length tracks was $\sigma(p_T)/p_T = 0.0058 p_T \oplus 0.0065 \oplus 0.0014/p_T$, with p_T in GeV.

The high-resolution uranium-scintillator calorimeter (CAL) [16–19] consisted of three parts: the forward (FCAL), the barrel (BCAL) and the rear (RCAL) calorimeters. Each part was subdivided transversely into towers and longitudinally into one electromagnetic section (EMC) and either one (in RCAL) or two (in BCAL and FCAL) hadronic sections (HAC). The smallest subdivision of the calorimeter was called a cell. The CAL energy resolutions, as measured under test-beam conditions, were $\sigma(E)/E = 0.18/\sqrt{E}$ for electrons and $\sigma(E)/E = 0.35/\sqrt{E}$ for hadrons, with E in GeV.

3. Data selection

Deep inelastic scattering events were selected by requiring that the outgoing positron was measured in the CAL. The scattered-positron identification was based on a neural-network algorithm using the CAL information [20].

For the reconstruction of the photon virtuality, Q^2, Bjorken x, and the $\gamma^* P$ centre-of-mass energy, W, the double angle (DA) method was chosen, in which the scattered-positron angle, θ_e, and the hadronic angle γ_H are used [21]. In the naive quark-parton model, γ_H is the angle of the scattered massless quark in the laboratory frame.

For each event, the measurement of the charged multiplicity was performed using tracks reconstructed in the CTD. The energy of the hadronic final state was measured using a combination of track and CAL information, excluding the cells and the track associated with the scattered positron. The selected tracks and CAL clusters were treated as massless Energy Flow Objects (EFOs) [22]. The clustering of objects was done according to the

---

[1]The ZEUS coordinate system is a right-handed Cartesian system, with the Z axis pointing in the proton beam direction, referred to as the "forward direction", and the X axis pointing left towards the centre of HERA. The coordinate origin is at the nominal interaction point.

Snowmass convention [23]. The transverse momentum, p_T, of each EFO was required to be greater than $0.15\,\text{GeV}$.

The event selection criteria were:

- $E_{e'} > 12\,\text{GeV}$, where $E_{e'}$ is the energy of the scattered positron, to select neutral current DIS events;

- $y_e \leq 0.95$, where y_e is the scaling variable y as determined from the energy and polar angle of the scattered positron. This cut reduces the photoproduction background;

- $y_{\text{JB}} \geq 0.04$, where y_{JB} is the estimate of y using the Jacquet-Blondel (JB) method [24]. It is defined as $y_{\text{JB}} = \sum_h (E_h - P_{Z_h})/2E_e$, where the sum runs over all EFOs and E_h and P_{Z_h} are the energies and longitudinal momenta of the EFOs respectively. This requirement guarantees sufficient accuracy for the DA reconstruction method;

- $35 \leq \delta \leq 60\,\text{GeV}$, where $\delta = \sum_i (E_i - P_{Z_i})$ and the sum runs over all EFOs and the scattered positron, to remove photoproduction events and events with large radiative corrections;

- $R \geq 25$ cm, where R is the distance from the beam axis to the impact position of the scattered positron on the face of the CAL. This ensured that the positron was fully contained within the detector and its position reconstructed with sufficient accuracy;

- $|Z_{\text{vtx}}| < 50$ cm, where Z_{vtx} is the longitudinal position of the vertex, to reduce background events from non-ep collisions.

To ensure high-quality tracks reconstructed with high efficiency, the following requirements were made:

- the tracks had to pass through at least three CTD superlayers;

- the tracks had to be associated with the primary event vertex;

- the tracks were restricted to the region $|\eta_{\text{LAB}}| \leq 1.75$, where η_{LAB} is the pseudorapidity of the tracks in the laboratory frame;

- the tracks had $p_T > 0.15$ GeV.

The analysis was restricted to the kinematic range $Q^2 > 25\,\text{GeV}^2$ and $70 < W < 225\,\text{GeV}$.

4. Analysis method

Due to the large asymmetry of the beam energies at HERA, a large fraction of the hadronic final state close to the proton direction lies outside the detector acceptance. Therefore only hadrons belonging to the current fragmentation regions of the HCM and Breit frames were used in this analysis. The boost to the corresponding reference frames was calculated using the positron four-momentum taken from the DA method.

4.1 Breit frame

In the Breit frame, which is defined by the condition that the momentum of the exchanged virtual boson is purely spacelike, $\mathbf{q} = (0, 0, -Q)$, the particles produced in the interaction can be assigned to one of two regions: the current region if their longitudinal momentum in the Breit frame is negative, and the target region if their longitudinal momentum is positive. The hadronic system of the current region used in this analysis is almost fully (about 95%) contained within the acceptance of the CTD.

Previous analyses compared the mean charged multiplicity $\langle n_{\rm ch} \rangle$ as a function of Q to $\langle n_{\rm ch} \rangle / 2$ as a function of $\sqrt{s}$ in $e^+ e^-$ collisions [2, 5]. For values of $Q > 8 \, \mathrm{GeV}$, reasonable agreement was observed, while some disagreement was found for $Q < 8 \, \mathrm{GeV}$. The difference can be understood in terms of higher-order processes [25], which change the available energy in the current region of the Breit frame, $E_{\rm B}^{\rm cr}$, which is no longer equal to $Q/2$. In this analysis the quantity $2 \cdot E_{\rm B}^{\rm cr}$ is used as a scale. On an event-by-event basis this method should compensate for particles and their corresponding energies migrating between current and target regions of the Breit frame.

4.2 Hadronic centre-of-mass frame

In the HCM frame, the exchanged virtual boson has four-momentum $\mathbf{q} = \{E, p\} = (\frac{W^2 - Q^2}{2W}, 0, 0, \frac{W^2 + Q^2}{2W})$. The hadronic final state is separated into the photon (current) and proton (target) fragmentation regions. About 60–80% of the current region of the HCM frame is contained within the acceptance of the CTD.

The multiplicity in the HCM frame in DIS is usually studied as a function of W [1, 8–10]. At HERA, the energy in the current region of the HCM frame, $E_{\rm HCM}^{\rm cr}$, coincides with $W/2$ within $0.3 - 0.4\%$. Thus, for practical reasons, W was used as the energy scale.

4.3 Invariant mass of the hadronic system

Charged multiplicities in the current region of both the Breit and HCM frames were also measured as functions of the invariant mass:

$$M_{\rm eff}^2 = \left(\sum_i E_i \right)^2 - \left(\sum_i P_{X_i} \right)^2 - \left(\sum_i P_{Y_i} \right)^2 - \left(\sum_i P_{Z_i} \right)^2, \qquad (4.1)$$

where the sum runs over all charged and neutral particles of the corresponding hadronic system.

5. Monte Carlo models, acceptance corrections and systematic errors

Samples of neutral current DIS events were generated using the colour-dipole model as implemented in Ariadne 4.12 [26] or with the MEPS model of Lepto 6.5 [27]. Both programs were interfaced to Heracles 4.6.1 [28, 29] using the Djangoh 1.1 [30, 31] program. Both Ariadne and Lepto use the Lund string model [32] for the hadronisation. The event samples were generated using the CTEQ4D [33] parametrisation of the parton distribution functions (PDFs) in the proton. The cluster hadronisation model as
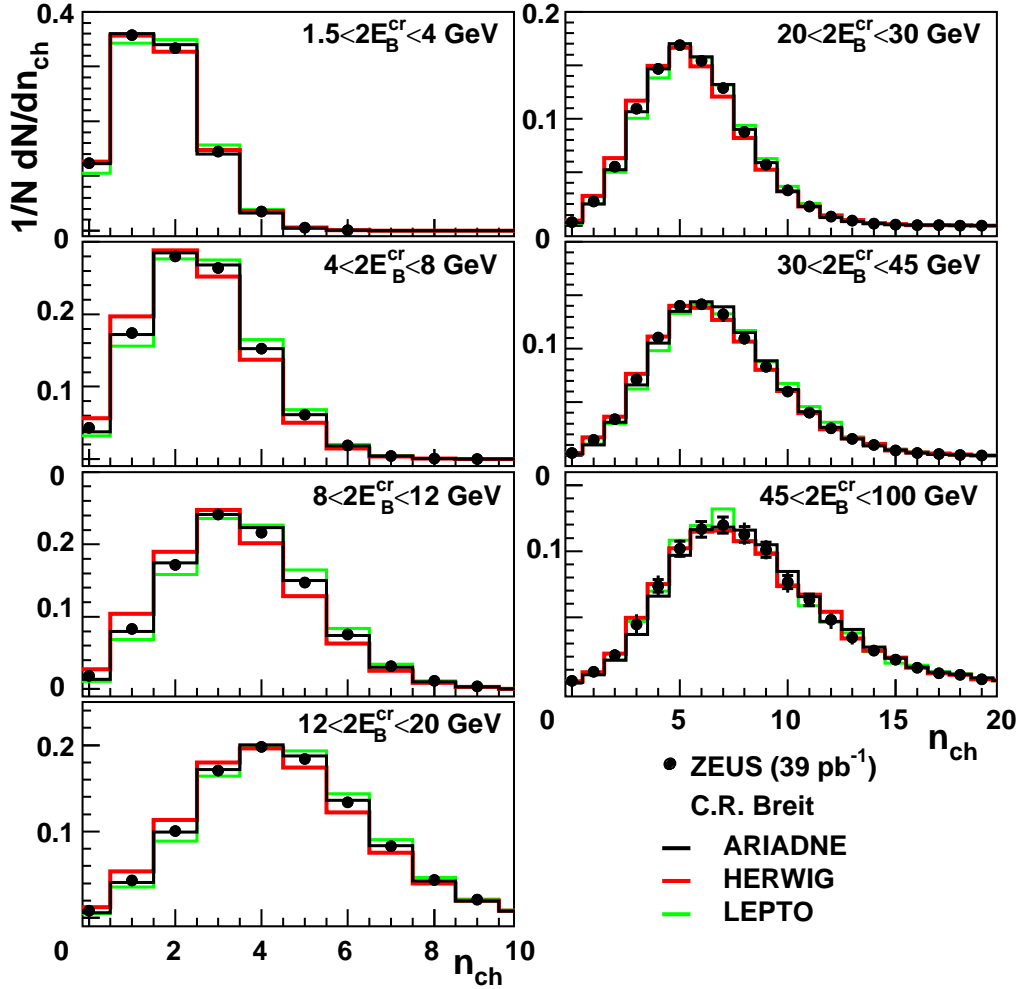
Figure 1: Multiplicity distributions measured in the current region of the Breit frame in bins of $2 \cdot E_{\mathrm{B}}^{\mathrm{cr}}$ (solid circles). The inner error bars represent the statistical uncertainties and the outer error bars the statistical and systematic uncertainties added in quadrature. The predictions (solid lines) of different MC models are also shown.

implemented in HERWIG 6.1 [34] was used to estimate the effect of different hadronisation schemes on the unfolding procedure. The minimum transverse momentum of outgoing partons in the hard interaction and of partons participating in multi-parton interactions is adjustable in HERWIG using the parameter p_T^{min}. The parameter was tuned in this analysis to improve the description of the detector distributions. The best agreement was found for $p_T^{\mathrm{min}} = 2.5\,\mathrm{GeV}$ [35]. The HERWIG samples were generated using CTEQ5L [36] parametrisation of the proton PDFs. The MC samples were used both for data correction and for comparison of the data to the model predictions.

The corrections applied to the data accounted for the effects of acceptance and resolution of the detector, event selection cuts, QED-radiative effects, track reconstruction, track selection cuts, and energy losses in the inactive material in front of the calorimeter in the case of the energy measurement. Finally the multiplicity distributions were corrected using a matrix unfolding method as described in earlier studies [5].

The generated events were passed through a full simulation of the detector, using a program based on GEANT 3.13 [37], and processed and selected with the same programs as used for the data. The simulated samples were used to determine the response of the detector and to evaluate the correction factors necessary to obtain hadron-level quantities. The hadron level is defined by those hadrons with lifetime $\tau \geq 3 \cdot 10^{-10}$ seconds. In order to compare the results to different experiments, corrections were calculated both including and not including the decay products of K_S^0 and Λ.

The dominant systematic uncertainty in this analysis arises from the simulation of the hadronic final state. To correct the data, the average of the correction factors from the ARIADNE and HERWIG MC programs was used. One half of the difference, as large as 5%, was assigned to the systematic uncertainties.

Other sources of uncertainty are (typical values of the uncertainties are shown in parentheses): event reconstruction and selection ($< 0.5\%$), track reconstruction and selection ($< 0.5\%$), and the uncertainty due to variation of the Q^2 cut by its resolution ($< 1.7\%$). The uncertainty due to contamination from diffractive events is negligible. The individual systematic uncertainties were added in quadrature. The major correlated uncertainty comes from the CAL energy scale ($< 1.5\%$) and is not shown in the figures or given in the tables. A detailed study of the sources contributing to the uncertainties of the measurement can be found elsewhere [38].

6. Results

6.1 Multiplicity distributions

The multiplicity distributions in the current region of the Breit frame are presented in figure 1 and table 1 and in figure 2 and table 2 in bins of $2 \cdot E_B^{cr}$ and in bins of M_{eff} respectively. The kinematic range of the analysis restricts the M_{eff} measurements in the current region of the Breit frame to a maximum value of about $20\,\text{GeV}$. The predictions of ARIADNE, LEPTO and HERWIG are also shown. All three MC models generally describe the data, but ARIADNE gives the best description. In all figures and tables the charged-particle decay products of K_S^0 and Λ are included, unless otherwise stated.

$2 \cdot E_{\mathrm{B}}^{\mathrm{cr}}$ (GeV)	1.5–4	4–8	8–12	12–20	20–30	30–45	45–100
$n_{\mathrm{ch}}=0$	$12.33 \pm 0.25^{+0.21}_{-0.23}$	$4.34 \pm 0.09^{+0.65}_{-0.65}$	$1.83 \pm 0.10^{+0.57}_{-0.56}$	$0.81 \pm 0.03^{+0.26}_{-0.26}$	$0.33 \pm 0.03^{+0.10}_{-0.10}$	$0.23 \pm 0.05^{+0.09}_{-0.09}$	$0.17 \pm 0.09^{+0.09}_{-0.09}$
1	$35.79 \pm 0.46^{+0.18}_{-0.35}$	$17.44 \pm 0.19^{+0.71}_{-0.72}$	$8.29 \pm 0.20^{+0.78}_{-0.77}$	$4.35 \pm 0.06^{+0.44}_{-0.44}$	$2.23 \pm 0.08^{+0.33}_{-0.33}$	$1.45 \pm 0.13^{+0.45}_{-0.44}$	$0.86 \pm 0.16^{+0.19}_{-0.20}$
2	$33.31 \pm 0.43^{+0.65}_{-0.57}$	$27.99 \pm 0.24^{+0.21}_{-0.21}$	$17.14 \pm 0.30^{+0.44}_{-0.51}$	$10.07 \pm 0.09^{+0.38}_{-0.38}$	$5.50 \pm 0.13^{+0.39}_{-0.38}$	$3.38 \pm 0.18^{+0.28}_{-0.27}$	$2.11 \pm 0.25^{+0.38}_{-0.35}$
3	$14.50 \pm 0.26^{+0.39}_{-0.39}$	$26.40 \pm 0.23^{+0.50}_{-0.49}$	$24.13 \pm 0.36^{+0.25}_{-0.37}$	$17.08 \pm 0.12^{+0.19}_{-0.20}$	$10.95 \pm 0.19^{+0.29}_{-0.32}$	$7.14 \pm 0.27^{+0.48}_{-0.42}$	$4.45 \pm 0.38^{+0.65}_{-0.63}$
4	$3.46 \pm 0.12^{+0.18}_{-0.18}$	$15.27 \pm 0.18^{+0.42}_{-0.42}$	$21.62 \pm 0.34^{+0.65}_{-0.66}$	$19.82 \pm 0.12^{+0.18}_{-0.27}$	$14.65 \pm 0.22^{+0.11}_{-0.21}$	$11.05 \pm 0.34^{+0.30}_{-0.25}$	$7.36 \pm 0.48^{+0.63}_{-0.60}$
5	$0.54 \pm 0.04^{+0.04}_{-0.03}$	$6.14 \pm 0.11^{+0.42}_{-0.40}$	$14.72 \pm 0.29^{+0.73}_{-0.71}$	$18.41 \pm 0.12^{+0.43}_{-0.45}$	$16.90 \pm 0.23^{+0.16}_{-0.15}$	$14.03 \pm 0.38^{+0.26}_{-0.25}$	$10.19 \pm 0.56^{+0.42}_{-0.33}$
6	$0.07 \pm 0.02^{+0.01}_{-0.01}$	$1.88 \pm 0.06^{+0.14}_{-0.14}$	$7.55 \pm 0.20^{+0.45}_{-0.40}$	$13.36 \pm 0.10^{+0.47}_{-0.48}$	$15.42 \pm 0.22^{+0.30}_{-0.30}$	$14.17 \pm 0.38^{+0.29}_{-0.36}$	$11.66 \pm 0.60^{+0.37}_{-0.27}$
7		$0.43 \pm 0.02^{+0.03}_{-0.03}$	$3.16 \pm 0.13^{+0.22}_{-0.19}$	$8.30 \pm 0.08^{+0.30}_{-0.26}$	$12.86 \pm 0.20^{+0.43}_{-0.41}$	$13.22 \pm 0.36^{+0.60}_{-0.61}$	$11.96 \pm 0.61^{+0.28}_{-0.16}$
8		$0.09 \pm 0.01^{+0.01}_{-0.01}$	$1.13 \pm 0.08^{+0.06}_{-0.08}$	$4.36 \pm 0.06^{+0.17}_{-0.10}$	$8.78 \pm 0.17^{+0.30}_{-0.30}$	$10.96 \pm 0.33^{+0.38}_{-0.44}$	$11.26 \pm 0.59^{+0.66}_{-0.52}$
9			$0.34 \pm 0.04^{+0.02}_{-0.02}$	$2.09 \pm 0.04^{+0.10}_{-0.06}$	$5.68 \pm 0.13^{+0.28}_{-0.28}$	$8.30 \pm 0.28^{+0.42}_{-0.41}$	$10.10 \pm 0.56^{+0.47}_{-0.44}$
10			$0.06 \pm 0.01^{+0.01}_{-0.01}$	$0.85 \pm 0.03^{+0.06}_{-0.04}$	$3.27 \pm 0.10^{+0.07}_{-0.02}$	$6.01 \pm 0.25^{+0.22}_{-0.08}$	$7.66 \pm 0.48^{+0.57}_{-0.65}$
11			$0.02 \pm 0.01^{+0.00}_{-0.00}$	$0.33 \pm 0.02^{+0.04}_{-0.03}$	$1.80 \pm 0.07^{+0.02}_{-0.05}$	$4.00 \pm 0.20^{+0.13}_{-0.07}$	$6.32 \pm 0.44^{+0.18}_{-0.27}$
12				$0.12 \pm 0.01^{+0.02}_{-0.02}$	$0.85 \pm 0.05^{+0.08}_{-0.09}$	$2.53 \pm 0.16^{+0.10}_{-0.09}$	$4.80 \pm 0.40^{+0.37}_{-0.57}$
13					$0.45 \pm 0.04^{+0.08}_{-0.07}$	$1.58 \pm 0.12^{+0.05}_{-0.07}$	$3.46 \pm 0.31^{+0.35}_{-0.41}$
14					$0.19 \pm 0.02^{+0.02}_{-0.02}$	$0.98 \pm 0.10^{+0.11}_{-0.11}$	$2.46 \pm 0.26^{+0.07}_{-0.13}$
15					$0.09 \pm 0.02^{+0.02}_{-0.02}$	$0.48 \pm 0.06^{+0.05}_{-0.02}$	$1.77 \pm 0.23^{+0.23}_{-0.37}$
16					$0.03 \pm 0.01^{+0.01}_{-0.01}$	$0.26 \pm 0.05^{+0.03}_{-0.03}$	$1.17 \pm 0.19^{+0.09}_{-0.11}$
17					$0.02 \pm 0.01^{+0.01}_{-0.02}$	$0.14 \pm 0.04^{+0.03}_{-0.04}$	$0.74 \pm 0.15^{+0.13}_{-0.14}$
18					$0.01 \pm 0.01^{+0.00}_{-0.00}$	$0.06 \pm 0.02^{+0.02}_{-0.02}$	$0.65 \pm 0.15^{+0.18}_{-0.07}$
19							$0.30 \pm 0.08^{+0.07}_{-0.11}$
20							$0.20 \pm 0.06^{+0.17}_{-0.05}$

Table 1: Multiplicity distributions $100 \cdot 1/N dN/dn_{ch}$ measured in the current region of the Breit frame in bins of $2 \cdot E_{\mathrm{B}}^{\mathrm{cr}}$. The first errors are statistical and the second are the systematic uncertainties.

| $M_{\rm eff}$ (GeV)	1.5–4	4–8	8–12	12–20
$n_{\rm ch}$=0	$1.90 \pm 0.05^{+0.34}_{-0.34}$	$0.23 \pm 0.04^{+0.07}_{-0.07}$	$0.04 \pm 0.02^{+0.02}_{-0.01}$	$0.02 \pm 0.02^{+0.01}_{-0.01}$
1	$9.81 \pm 0.13^{+0.47}_{-0.50}$	$1.68 \pm 0.12^{+0.24}_{-0.22}$	$0.40 \pm 0.05^{+0.02}_{-0.02}$	$0.13 \pm 0.05^{+0.02}_{-0.02}$
2	$21.73 \pm 0.20^{+0.28}_{-0.32}$	$5.57 \pm 0.24^{+0.31}_{-0.26}$	$1.26 \pm 0.09^{+0.04}_{-0.07}$	$0.56 \pm 0.13^{+0.21}_{-0.21}$
3	$28.19 \pm 0.23^{+0.28}_{-0.29}$	$12.12 \pm 0.37^{+0.35}_{-0.24}$	$3.58 \pm 0.16^{+0.16}_{-0.14}$	$1.49 \pm 0.18^{+0.19}_{-0.17}$
4	$21.12 \pm 0.20^{+0.15}_{-0.14}$	$17.68 \pm 0.47^{+0.31}_{-0.40}$	$6.73 \pm 0.23^{+0.09}_{-0.12}$	$3.33 \pm 0.30^{+0.26}_{-0.30}$
5	$10.93 \pm 0.14^{+0.32}_{-0.25}$	$19.78 \pm 0.51^{+0.21}_{-0.29}$	$11.07 \pm 0.31^{+0.34}_{-0.37}$	$5.64 \pm 0.39^{+0.27}_{-0.18}$
6	$4.40 \pm 0.09^{+0.13}_{-0.08}$	$17.11 \pm 0.48^{+0.69}_{-0.69}$	$14.17 \pm 0.37^{+0.11}_{-0.20}$	$8.38 \pm 0.50^{+0.24}_{-0.12}$
7	$1.43 \pm 0.05^{+0.05}_{-0.03}$	$12.41 \pm 0.41^{+0.17}_{-0.18}$	$16.01 \pm 0.40^{+0.39}_{-0.42}$	$10.47 \pm 0.58^{+0.40}_{-0.35}$
8	$0.38 \pm 0.02^{+0.02}_{-0.01}$	$7.27 \pm 0.31^{+0.25}_{-0.24}$	$14.40 \pm 0.38^{+0.46}_{-0.46}$	$12.16 \pm 0.66^{+0.43}_{-0.42}$
9	$0.09 \pm 0.01^{+0.01}_{-0.01}$	$3.51 \pm 0.23^{+0.47}_{-0.46}$	$11.74 \pm 0.35^{+0.29}_{-0.26}$	$12.75 \pm 0.68^{+0.27}_{-0.17}$
10		$1.63 \pm 0.15^{+0.17}_{-0.16}$	$8.46 \pm 0.30^{+0.33}_{-0.29}$	$11.80 \pm 0.69^{+0.28}_{-0.26}$
11		$0.66 \pm 0.09^{+0.09}_{-0.08}$	$5.50 \pm 0.24^{+0.25}_{-0.21}$	$10.03 \pm 0.63^{+0.33}_{-0.12}$
12		$0.26 \pm 0.06^{+0.05}_{-0.05}$	$3.16 \pm 0.18^{+0.32}_{-0.31}$	$7.74 \pm 0.57^{+0.25}_{-0.34}$
13		$0.04 \pm 0.02^{+0.01}_{-0.01}$	$1.76 \pm 0.13^{+0.24}_{-0.20}$	$5.56 \pm 0.46^{+0.21}_{-0.48}$
14		$0.03 \pm 0.02^{+0.01}_{-0.01}$	$0.94 \pm 0.09^{+0.13}_{-0.11}$	$4.02 \pm 0.40^{+0.33}_{-0.21}$
15		$0.01 \pm 0.01^{+0.01}_{-0.01}$	$0.41 \pm 0.06^{+0.13}_{-0.12}$	$2.50 \pm 0.31^{+0.11}_{-0.22}$
16			$0.19 \pm 0.04^{+0.04}_{-0.04}$	$1.44 \pm 0.25^{+0.07}_{-0.14}$
17			$0.10 \pm 0.03^{+0.03}_{-0.05}$	$0.89 \pm 0.19^{+0.21}_{-0.23}$
18			$0.05 \pm 0.02^{+0.03}_{-0.02}$	$0.52 \pm 0.14^{+0.13}_{-0.13}$
19			$0.01 \pm 0.01^{+0.00}_{-0.00}$	$0.22 \pm 0.09^{+0.11}_{-0.11}$
20				$0.19 \pm 0.09^{+0.13}_{-0.10}$

Table 2: Multiplicity distributions $100 \cdot 1/N dN/dn_{ch}$ measured in the current region of the Breit frame in bins of $M_{\rm eff}$. The first errors are statistical and the second are the systematic uncertainties.

For a given bin of energy, the multiplicities as a function of $2 \cdot E_{\rm B}^{\rm cr}$ and $M_{\rm eff}$ differ by approximately a factor of two. This is due to the fact that $2 \cdot E_{\rm B}^{\rm cr}$ (as well as Q or W) characterise the total centre-of-mass energy of the system of which only one hemisphere is measured. On the other hand the $M_{\rm eff}$ method measures the multiplicity of the system with respect to the corresponding invariant mass.

The multiplicity distributions in the current region of the HCM frame are presented in figure 3 and table 3 in bins of W. Both ARIADNE and LEPTO predict similar W distributions and give a reasonable description of the data. HERWIG predicts longer tails for the multiplicity distributions in bins of W. This leads to higher average multiplicities, affecting the unfolded multiplicity values and increasing the systematic uncertainties of the measurement. The ARIADNE predictions vary slightly from both LEPTO and HERWIG at the rising edge of the distributions, which also leads to an increase of the systematic uncertainties.

The multiplicity distributions in the current region of the HCM frame in bins of $M_{\rm eff}$ are presented in figure 4 and table 4. To minimise the extrapolation both in multiplicity and $M_{\rm eff}$, an additional requirement, $|\eta_{\rm LAB}| < 1.75$, was applied at the hadron level. None of the MC models shown in figure 4 give a complete description of the data. This is most visible at higher values of $M_{\rm eff}$.
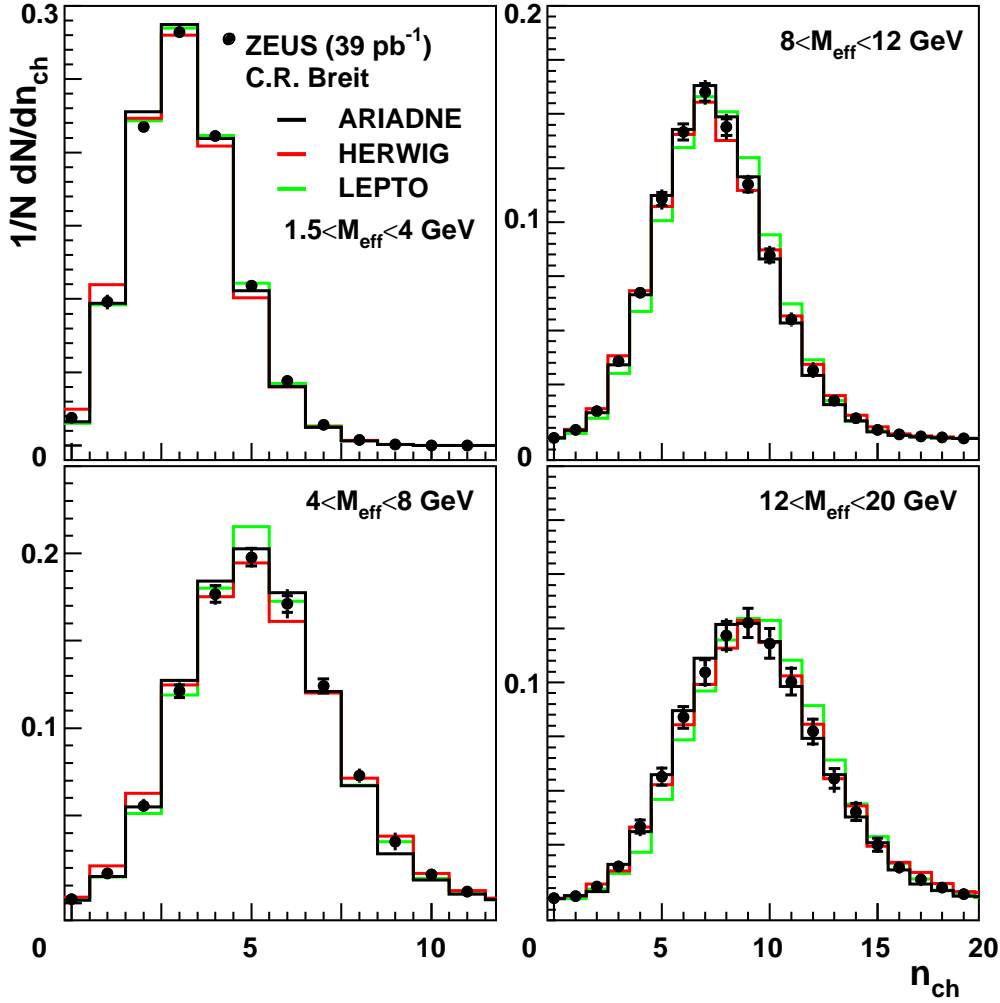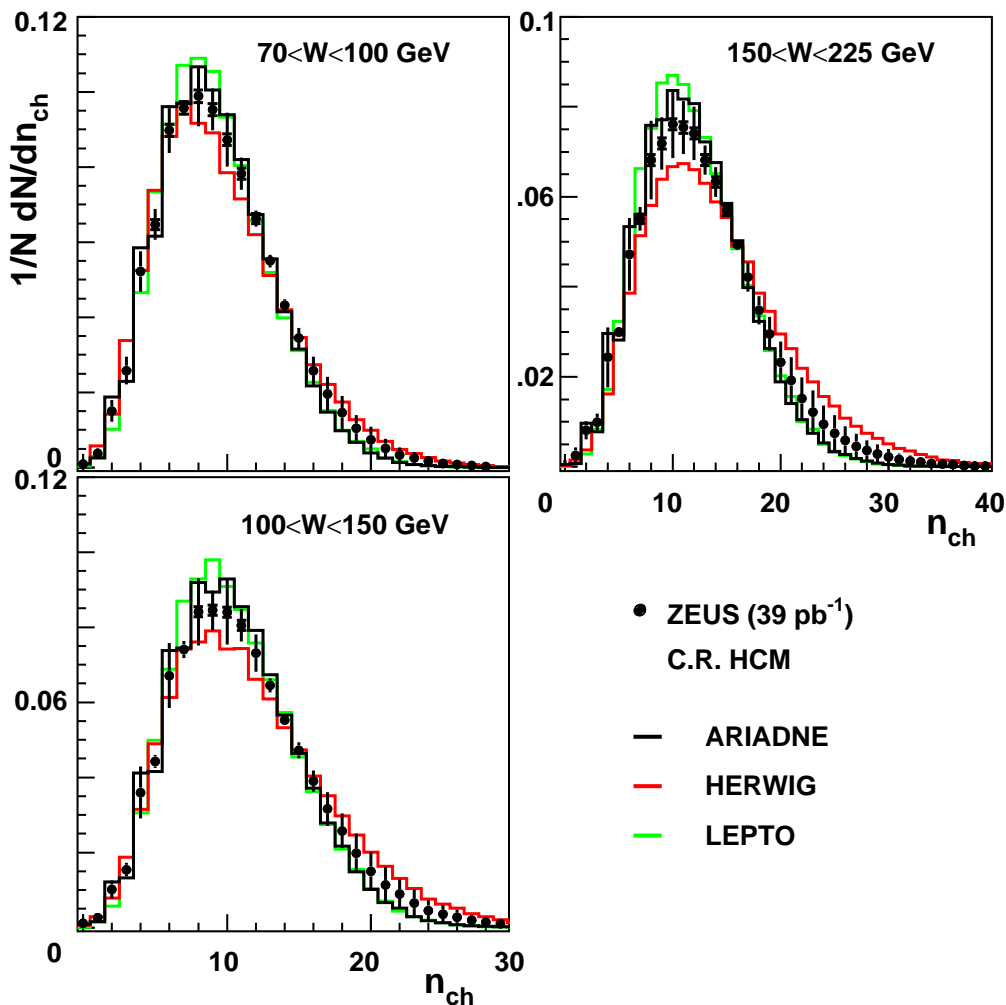
Figure 2: Multiplicity distributions measured in the current region of the Breit frame in bins of $M_{\rm eff}$ (solid circles). The inner error bars represent the statistical uncertainties and the outer error bars the statistical and systematic uncertainties added in quadrature. The predictions (solid lines) of different MC models are also shown.

6.2 KNO scaling

The multiplicity distributions are expected to scale with energy as discussed in detail elsewhere [39]. A commonly used form of the scaling, from KNO [40], is shown in figures 5–8, where the product of the multiplicity distribution $P(n_{\rm ch})$ with average multiplicity $\langle n_{\rm ch}\rangle$, $\langle n_{\rm ch}\rangle P(n_{\rm ch})$, is shown as a function of $n_{\rm ch}/\langle n_{\rm ch}\rangle$.

In figure 5(a), the KNO distributions measured in bins of W in the current region of the HCM frame are shown. Within the uncertainties, the distributions measured in three bins of W agree. They also agree well with the average distribution, which was calculated

ZEUS

Figure 3: Multiplicity distributions measured in the current region of the HCM frame in bins of W (solid circles). The inner error bars represent the statistical uncertainties and the outer error bars the statistical and systematic uncertainties added in quadrature. The predictions (solid lines) of different MC models are also shown.

using data for the entire W region, $70 < W < 225\,\text{GeV}$. This average KNO spectrum, presented as a histogram, is shown in figures 5 and 6 as a reference KNO distribution.

The reference KNO distribution is compared to the measurements in the current region of the Breit frame in figures 5(b) and 5(c) in bins of $2 \cdot E_{\text{B}}^{\text{cr}}$. For values of $2 \cdot E_{\text{B}}^{\text{cr}} > 12\,\text{GeV}$, as shown in figure 5(c), the measurements are in reasonable agreement with the reference KNO histogram. For lower values of $2 \cdot E_{\text{B}}^{\text{cr}}$, as demonstrated in figure 5(b), the distributions do not follow the KNO-scaling behaviour; they have different shapes, but approach the KNO curve with increasing values of $2 \cdot E_{\text{B}}^{\text{cr}}$.

W (GeV)	70–100	100–150	150–225
n_{ch}=0	$0.09 \pm 0.03^{+0.01}_{-0.01}$	$0.11 \pm 0.03^{+0.02}_{-0.02}$	$0.09 \pm 0.02^{+0.05}_{-0.04}$
1	$0.37 \pm 0.04^{+0.13}_{-0.13}$	$0.26 \pm 0.03^{+0.10}_{-0.10}$	$0.25 \pm 0.04^{+0.17}_{-0.17}$
2	$1.50 \pm 0.07^{+0.28}_{-0.28}$	$1.02 \pm 0.06^{+0.23}_{-0.23}$	$0.81 \pm 0.05^{+0.19}_{-0.19}$
3	$2.58 \pm 0.09^{+0.36}_{-0.36}$	$1.55 \pm 0.06^{+0.17}_{-0.17}$	$0.99 \pm 0.05^{+0.18}_{-0.17}$
4	$5.22 \pm 0.13^{+0.52}_{-0.52}$	$3.60 \pm 0.09^{+0.69}_{-0.69}$	$2.43 \pm 0.08^{+0.66}_{-0.66}$
5	$6.47 \pm 0.14^{+0.39}_{-0.38}$	$4.43 \pm 0.10^{+0.14}_{-0.13}$	$3.00 \pm 0.08^{+0.07}_{-0.06}$
6	$8.97 \pm 0.16^{+0.58}_{-0.58}$	$6.71 \pm 0.12^{+0.85}_{-0.85}$	$4.72 \pm 0.10^{+0.80}_{-0.80}$
7	$9.57 \pm 0.17^{+0.12}_{-0.09}$	$7.40 \pm 0.13^{+0.19}_{-0.18}$	$5.51 \pm 0.11^{+0.24}_{-0.23}$
8	$9.89 \pm 0.16^{+0.78}_{-0.78}$	$8.41 \pm 0.13^{+0.89}_{-0.89}$	$6.82 \pm 0.12^{+0.87}_{-0.87}$
9	$9.53 \pm 0.16^{+0.53}_{-0.53}$	$8.45 \pm 0.13^{+0.51}_{-0.51}$	$7.18 \pm 0.12^{+0.57}_{-0.57}$
10	$8.73 \pm 0.16^{+0.70}_{-0.70}$	$8.40 \pm 0.13^{+0.85}_{-0.85}$	$7.61 \pm 0.13^{+0.74}_{-0.74}$
11	$7.82 \pm 0.15^{+0.41}_{-0.41}$	$8.05 \pm 0.13^{+0.40}_{-0.41}$	$7.54 \pm 0.13^{+0.57}_{-0.57}$
12	$6.63 \pm 0.14^{+0.16}_{-0.16}$	$7.31 \pm 0.12^{+0.49}_{-0.49}$	$7.41 \pm 0.13^{+0.58}_{-0.58}$
13	$5.50 \pm 0.13^{+0.11}_{-0.12}$	$6.46 \pm 0.12^{+0.15}_{-0.15}$	$6.82 \pm 0.12^{+0.30}_{-0.30}$
14	$4.32 \pm 0.12^{+0.12}_{-0.15}$	$5.53 \pm 0.11^{+0.03}_{-0.02}$	$6.33 \pm 0.12^{+0.31}_{-0.31}$
15	$3.45 \pm 0.11^{+0.25}_{-0.25}$	$4.72 \pm 0.10^{+0.19}_{-0.19}$	$5.69 \pm 0.11^{+0.05}_{-0.05}$
16	$2.58 \pm 0.09^{+0.37}_{-0.37}$	$3.90 \pm 0.10^{+0.27}_{-0.27}$	$4.93 \pm 0.11^{+0.00}_{-0.03}$
17	$1.96 \pm 0.09^{+0.44}_{-0.44}$	$3.16 \pm 0.09^{+0.44}_{-0.44}$	$4.22 \pm 0.10^{+0.30}_{-0.30}$
18	$1.46 \pm 0.08^{+0.45}_{-0.45}$	$2.58 \pm 0.08^{+0.45}_{-0.45}$	$3.48 \pm 0.09^{+0.30}_{-0.30}$
19	$1.05 \pm 0.07^{+0.35}_{-0.35}$	$1.98 \pm 0.08^{+0.51}_{-0.51}$	$2.95 \pm 0.09^{+0.37}_{-0.37}$
20	$0.74 \pm 0.06^{+0.34}_{-0.34}$	$1.50 \pm 0.07^{+0.51}_{-0.51}$	$2.32 \pm 0.08^{+0.45}_{-0.45}$
21	$0.51 \pm 0.06^{+0.25}_{-0.25}$	$1.14 \pm 0.06^{+0.48}_{-0.48}$	$1.91 \pm 0.08^{+0.52}_{-0.52}$
22	$0.34 \pm 0.05^{+0.19}_{-0.19}$	$0.90 \pm 0.06^{+0.38}_{-0.38}$	$1.51 \pm 0.07^{+0.48}_{-0.48}$
23	$0.25 \pm 0.05^{+0.16}_{-0.16}$	$0.65 \pm 0.05^{+0.36}_{-0.36}$	$1.22 \pm 0.07^{+0.47}_{-0.47}$
24	$0.17 \pm 0.04^{+0.12}_{-0.12}$	$0.46 \pm 0.05^{+0.27}_{-0.27}$	$0.94 \pm 0.06^{+0.41}_{-0.41}$
25	$0.10 \pm 0.04^{+0.08}_{-0.08}$	$0.36 \pm 0.05^{+0.23}_{-0.23}$	$0.74 \pm 0.06^{+0.40}_{-0.40}$
26	$0.08 \pm 0.03^{+0.06}_{-0.06}$	$0.28 \pm 0.04^{+0.20}_{-0.20}$	$0.58 \pm 0.05^{+0.31}_{-0.31}$
27	$0.05 \pm 0.03^{+0.04}_{-0.04}$	$0.19 \pm 0.04^{+0.15}_{-0.15}$	$0.45 \pm 0.05^{+0.27}_{-0.27}$
28	$0.03 \pm 0.02^{+0.03}_{-0.03}$	$0.15 \pm 0.04^{+0.12}_{-0.12}$	$0.36 \pm 0.05^{+0.23}_{-0.23}$
29	$0.02 \pm 0.02^{+0.01}_{-0.02}$	$0.10 \pm 0.04^{+0.08}_{-0.08}$	$0.29 \pm 0.05^{+0.20}_{-0.20}$
30	$0.01 \pm 0.03^{+0.01}_{-0.02}$	$0.07 \pm 0.02^{+0.05}_{-0.05}$	$0.22 \pm 0.05^{+0.17}_{-0.17}$
31		$0.05 \pm 0.03^{+0.04}_{-0.04}$	$0.17 \pm 0.04^{+0.12}_{-0.12}$
32		$0.04 \pm 0.03^{+0.03}_{-0.03}$	$0.13 \pm 0.05^{+0.11}_{-0.11}$
33		$0.03 \pm 0.03^{+0.03}_{-0.03}$	$0.10 \pm 0.04^{+0.08}_{-0.08}$
34		$0.01 \pm 0.02^{+0.01}_{-0.01}$	$0.08 \pm 0.03^{+0.06}_{-0.06}$
35		$0.01 \pm 0.01^{+0.01}_{-0.01}$	$0.05 \pm 0.03^{+0.05}_{-0.07}$
36			$0.05 \pm 0.03^{+0.05}_{-0.04}$
37			$0.03 \pm 0.03^{+0.03}_{-0.03}$
38			$0.02 \pm 0.02^{+0.02}_{-0.02}$

Table 3: Multiplicity distributions $100 \cdot 1/N dN/dn_{ch}$ measured in the current region of the HCM in bins of W. The first errors are statistical and the second are the systematic uncertainties.

In figure 6, the KNO distributions measured in bins of M_{eff} in the current region of the HCM frame are presented. The multiplicity distributions in bins of M_{eff} do not follow the same KNO scaling observed for measurements as functions of W or $2 \cdot E_{\mathrm{B}}^{\mathrm{cr}}$, but do demonstrate scaling behaviour for M_{eff} values above 8 GeV. The measurements at
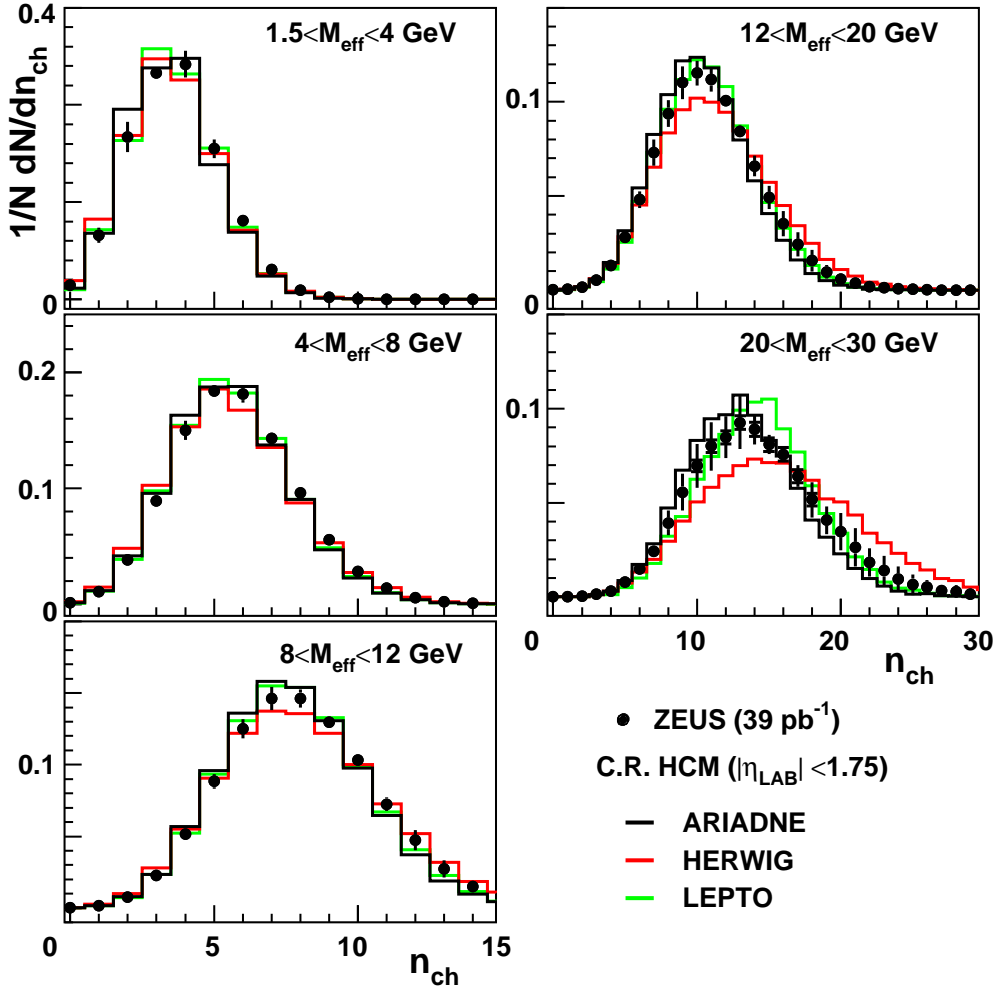
Figure 4: Multiplicity distributions measured in the current region of the HCM frame in bins of $M_{\rm eff}$ (solid circles). The inner error bars represent the statistical uncertainties and the outer error bars the statistical and systematic uncertainties added in quadrature. The predictions (solid lines) of different MC models are also shown.

$M_{\rm eff} < 4\,{\rm GeV}$ in the current regions of both the Breit and HCM frames behave differently from the measurements at the higher values of $M_{\rm eff}$.

Figure 7 shows a comparison of the KNO distributions from ZEUS with results obtained in e^+e^- collisions. The measurements in bins of $2 \cdot E_{\rm B}^{\rm cr}$, for $2 \cdot E_{\rm B}^{\rm cr} > 12\,{\rm GeV}$, and in bins of W are plotted together and compared with measurements in one hemisphere of e^+e^-. In figure 7(a), a comparison with results from the TASSO collaboration [41] in the energy range $14 < \sqrt{s_{\rm ee}} < 44\,{\rm GeV}$ is shown. At LEP only DELPHI [42] and OPAL [43] performed measurements in a single hemisphere at $\sqrt{s_{\rm ee}} = 91.2\,{\rm GeV}$. A comparison with

M_{eff} (GeV)	1.5–4	4–8	8–12	12–20	20–30
n_{ch}=0	$1.44 \pm 0.09^{+0.58}_{-0.58}$	$0.12 \pm 0.01^{+0.04}_{-0.04}$	$0.02 \pm 0.01^{+0.00}_{-0.00}$		
1	$6.59 \pm 0.22^{+0.74}_{-0.74}$	$1.06 \pm 0.04^{+0.05}_{-0.06}$	$0.18 \pm 0.02^{+0.03}_{-0.03}$	$0.05 \pm 0.01^{+0.01}_{-0.01}$	
2	$16.69 \pm 0.40^{+1.54}_{-1.50}$	$3.83 \pm 0.09^{+0.13}_{-0.13}$	$0.76 \pm 0.04^{+0.01}_{-0.04}$	$0.17 \pm 0.02^{+0.01}_{-0.01}$	$0.03 \pm 0.02^{+0.01}_{-0.01}$
3	$23.29 \pm 0.49^{+0.27}_{-0.21}$	$8.91 \pm 0.14^{+0.27}_{-0.22}$	$2.27 \pm 0.08^{+0.03}_{-0.10}$	$0.54 \pm 0.04^{+0.01}_{-0.03}$	$0.13 \pm 0.04^{+0.05}_{-0.03}$
4	$24.20 \pm 0.52^{+1.26}_{-1.28}$	$15.01 \pm 0.19^{+0.81}_{-0.82}$	$5.15 \pm 0.12^{+0.32}_{-0.38}$	$1.32 \pm 0.06^{+0.08}_{-0.09}$	$0.31 \pm 0.06^{+0.08}_{-0.06}$
5	$15.49 \pm 0.41^{+0.87}_{-0.86}$	$18.40 \pm 0.21^{+0.14}_{-0.21}$	$8.84 \pm 0.16^{+0.46}_{-0.48}$	$2.81 \pm 0.09^{+0.19}_{-0.20}$	$0.78 \pm 0.10^{+0.10}_{-0.07}$
6	$8.07 \pm 0.29^{+0.34}_{-0.32}$	$18.13 \pm 0.22^{+0.71}_{-0.71}$	$12.51 \pm 0.19^{+0.64}_{-0.65}$	$4.81 \pm 0.12^{+0.41}_{-0.43}$	$1.49 \pm 0.13^{+0.13}_{-0.07}$
7	$3.03 \pm 0.17^{+0.16}_{-0.18}$	$14.32 \pm 0.19^{+0.32}_{-0.34}$	$14.61 \pm 0.21^{+0.79}_{-0.79}$	$7.30 \pm 0.15^{+0.68}_{-0.69}$	$2.43 \pm 0.18^{+0.18}_{-0.23}$
8	$0.95 \pm 0.09^{+0.13}_{-0.12}$	$9.62 \pm 0.16^{+0.26}_{-0.24}$	$14.62 \pm 0.21^{+0.60}_{-0.59}$	$9.38 \pm 0.18^{+0.68}_{-0.69}$	$3.91 \pm 0.22^{+0.65}_{-0.59}$
9	$0.20 \pm 0.04^{+0.06}_{-0.07}$	$5.54 \pm 0.12^{+0.50}_{-0.49}$	$12.97 \pm 0.20^{+0.20}_{-0.16}$	$11.03 \pm 0.19^{+0.85}_{-0.86}$	$5.56 \pm 0.28^{+0.95}_{-0.93}$
10	$0.05 \pm 0.02^{+0.03}_{-0.01}$	$2.82 \pm 0.09^{+0.34}_{-0.33}$	$10.32 \pm 0.19^{+0.28}_{-0.27}$	$11.53 \pm 0.20^{+0.63}_{-0.63}$	$6.97 \pm 0.31^{+1.10}_{-1.13}$
11		$1.36 \pm 0.06^{+0.28}_{-0.28}$	$7.24 \pm 0.16^{+0.46}_{-0.44}$	$11.18 \pm 0.20^{+0.59}_{-0.59}$	$8.01 \pm 0.33^{+1.23}_{-1.25}$
12		$0.57 \pm 0.04^{+0.13}_{-0.13}$	$4.74 \pm 0.13^{+0.71}_{-0.70}$	$10.07 \pm 0.20^{+0.20}_{-0.21}$	$8.48 \pm 0.35^{+1.05}_{-1.04}$
13		$0.19 \pm 0.03^{+0.07}_{-0.07}$	$2.73 \pm 0.10^{+0.59}_{-0.58}$	$8.44 \pm 0.18^{+0.27}_{-0.24}$	$9.26 \pm 0.36^{+1.36}_{-1.36}$
14		$0.08 \pm 0.02^{+0.02}_{-0.02}$	$1.51 \pm 0.08^{+0.38}_{-0.37}$	$6.58 \pm 0.16^{+0.52}_{-0.51}$	$8.90 \pm 0.38^{+0.72}_{-0.71}$
15		$0.03 \pm 0.01^{+0.00}_{-0.01}$	$0.83 \pm 0.06^{+0.28}_{-0.28}$	$4.92 \pm 0.15^{+0.60}_{-0.59}$	$8.09 \pm 0.36^{+0.37}_{-0.35}$
16			$0.35 \pm 0.04^{+0.14}_{-0.14}$	$3.53 \pm 0.13^{+0.66}_{-0.65}$	$7.57 \pm 0.36^{+0.21}_{-0.21}$
17			$0.20 \pm 0.03^{+0.08}_{-0.08}$	$2.43 \pm 0.11^{+0.64}_{-0.63}$	$6.41 \pm 0.35^{+0.47}_{-0.45}$
18			$0.08 \pm 0.02^{+0.03}_{-0.03}$	$1.56 \pm 0.10^{+0.56}_{-0.56}$	$5.17 \pm 0.33^{+0.86}_{-0.90}$
19			$0.03 \pm 0.02^{+0.02}_{-0.02}$	$0.96 \pm 0.08^{+0.36}_{-0.36}$	$4.08 \pm 0.29^{+0.65}_{-0.71}$
20			$0.01 \pm 0.01^{+0.01}_{-0.01}$	$0.59 \pm 0.06^{+0.25}_{-0.25}$	$3.47 \pm 0.29^{+0.96}_{-0.95}$
21				$0.36 \pm 0.05^{+0.18}_{-0.18}$	$2.63 \pm 0.27^{+0.99}_{-0.98}$
22				$0.18 \pm 0.04^{+0.12}_{-0.11}$	$1.83 \pm 0.24^{+0.72}_{-0.72}$
23				$0.12 \pm 0.04^{+0.09}_{-0.08}$	$1.39 \pm 0.23^{+0.77}_{-0.75}$
24				$0.07 \pm 0.02^{+0.04}_{-0.04}$	$0.96 \pm 0.20^{+0.62}_{-0.63}$
25				$0.04 \pm 0.02^{+0.02}_{-0.02}$	$0.66 \pm 0.20^{+0.50}_{-0.52}$
26				$0.02 \pm 0.02^{+0.01}_{-0.02}$	$0.53 \pm 0.16^{+0.33}_{-0.33}$
27					$0.34 \pm 0.16^{+0.27}_{-0.22}$
28					$0.28 \pm 0.20^{+0.26}_{-0.26}$
29					$0.13 \pm 0.11^{+0.11}_{-0.13}$
30					$0.09 \pm 0.07^{+0.07}_{-0.12}$

Table 4: Multiplicity distributions $100 \cdot 1/N dN/dn_{ch}$ measured in the current region of the HCM frame in bins of M_{eff}. The first errors are statistical and the second are the systematic uncertainties.

the present data is shown in figure 7(b). The systematic uncertainties are not shown, but within statistical uncertainties there is a remarkable agreement between ep and e^+e^- results. However, the LEP data differ somewhat from the present measurement in the peak region and at very low values of $n_{\text{ch}}/\langle n_{\text{ch}}\rangle$.

The data as a function of M_{eff}, for $M_{\text{eff}} > 8\,\text{GeV}$, are compared with the e^+e^- measurements for the whole event in figure 8. Both the TASSO and LEP [42–56] data ($91.2 < \sqrt{s_{\text{ee}}} < 209\,\text{GeV}$) agree with the present measurement.

6.3 Mean charged multiplicity

Figure 9 and table 5 show the mean charged multiplicity, $\langle n_{\text{ch}}\rangle$, in the current region of
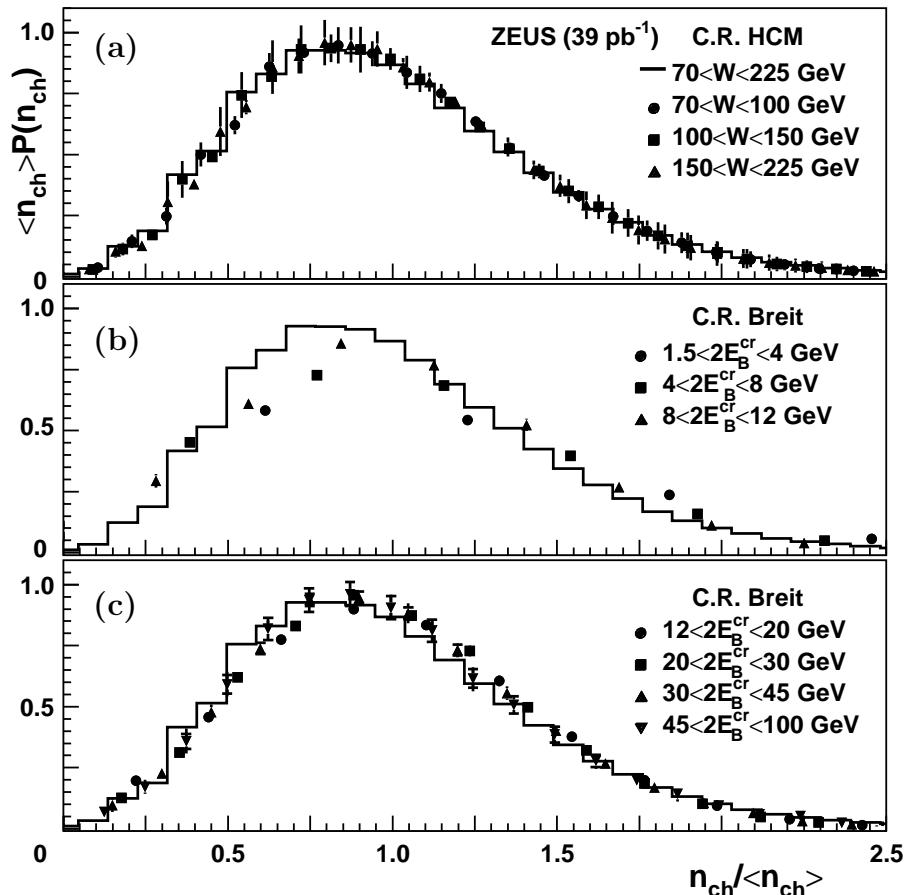
ZEUS

Figure 5: The multiplicity distributions plotted in KNO form. The reference KNO histogram represents the measured distribution in the HCM frame in the entire W range. (a) Multiplicity distributions measured in the current region of the HCM frame in bins of W. Multiplicity distributions measured in the current region of the Breit frame in bins of $2 \cdot E_{\mathrm{B}}^{\mathrm{cr}}$ for (b) $1.5 < 2 \cdot E_{\mathrm{B}}^{\mathrm{cr}} < 12$ GeV and (c) $12 < 2 \cdot E_{\mathrm{B}}^{\mathrm{cr}} < 100$ GeV.

the HCM frame as a function of W and the mean charged multiplicity in the current region of the Breit frame as a function of $2 \cdot E_{\mathrm{B}}^{\mathrm{cr}}$. The K_S^0 and Λ hadrons were considered stable in figure 9, where the data are compared with results of previously published HERA measurements [1, 2, 4, 5]. As expected, at low values of $2 \cdot E_{\mathrm{B}}^{\mathrm{cr}}$, the measurement differs with those as a function of Q (see section 4.1). At higher values of $2 \cdot E_{\mathrm{B}}^{\mathrm{cr}}$ the data agree within the experimental uncertainties with the previous ZEUS and H1 measurements, but lie systematically above them. The data are in good agreement with the ARIADNE and LEPTO predictions. The HERWIG predictions also describe the data but are below those from ARIADNE and LEPTO. In the current region of the HCM, the measurement agrees well, with improved statistical and systematic uncertainties, with the earlier H1 results. The ARIADNE and LEPTO predictions agree with the data. HERWIG predicts a very different slope, with much higher multiplicities at higher energies; with increasing energy the agreement with data degrades.

ZEUS
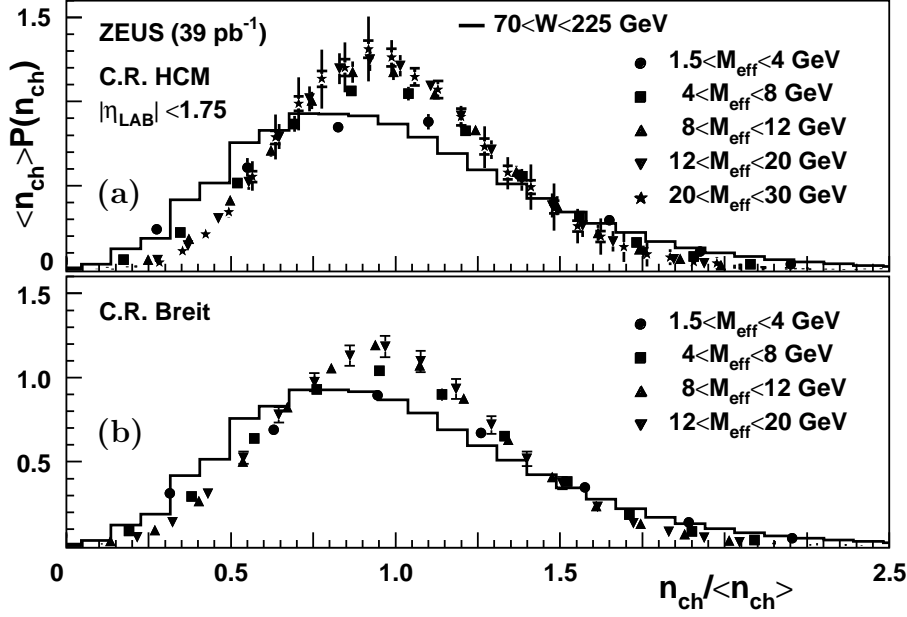
Figure 6: The multiplicity distributions plotted in KNO form and compared to the reference KNO distribution (histogram). The multiplicity distributions are measured in bins of M_{eff} in the current regions of (a) the HCM frame, restricted in η_{LAB}, and (b) the Breit frame.

$2 \cdot E_{\text{B}}^{\text{cr}}$ (GeV)	$\langle n_{\text{ch}} \rangle$ (K^0, Λ stable)	$\langle n_{\text{ch}} \rangle$ (K^0, Λ decay)
2.9	$1.50 \pm 0.01^{+0.04}_{-0.00}$	$1.63 \pm 0.01^{+0.05}_{-0.01}$
5.9	$2.39 \pm 0.01^{+0.09}_{-0.05}$	$2.60 \pm 0.01^{+0.11}_{-0.05}$
9.6	$3.27 \pm 0.01^{+0.12}_{-0.08}$	$3.55 \pm 0.01^{+0.15}_{-0.08}$
14.8	$4.17 \pm 0.01^{+0.10}_{-0.05}$	$4.53 \pm 0.01^{+0.12}_{-0.05}$
23.8	$5.22 \pm 0.01^{+0.06}_{-0.05}$	$5.67 \pm 0.01^{+0.08}_{-0.05}$
35.6	$6.19 \pm 0.03^{+0.08}_{-0.07}$	$6.68 \pm 0.03^{+0.08}_{-0.08}$
58.1	$7.46 \pm 0.06^{+0.14}_{-0.16}$	$8.04 \pm 0.06^{+0.16}_{-0.18}$
W (GeV)	$\langle n_{\text{ch}} \rangle$ (K^0, Λ stable)	$\langle n_{\text{ch}} \rangle$ (K^0, Λ decay)
84.6	$8.72 \pm 0.02^{+0.22}_{-0.22}$	$9.58 \pm 0.02^{+0.33}_{-0.33}$
123.8	$10.04 \pm 0.02^{+0.44}_{-0.44}$	$11.07 \pm 0.02^{+0.61}_{-0.61}$
184.5	$11.40 \pm 0.03^{+0.58}_{-0.58}$	$12.59 \pm 0.03^{+0.79}_{-0.79}$

Table 5: Mean charged multiplicity, $\langle n_{\text{ch}} \rangle$, measured in the current region of the Breit frame as a function of $2 \cdot E_{\text{B}}^{\text{cr}}$ and in the current fragmentation region of the HCM frame as a function of W. The first errors are statistical and the second are the systematic uncertainties.

The mean charged multiplicities in the current regions of the Breit and HCM frames are presented in figure 10 and table 6 as a function of the invariant mass of the corresponding
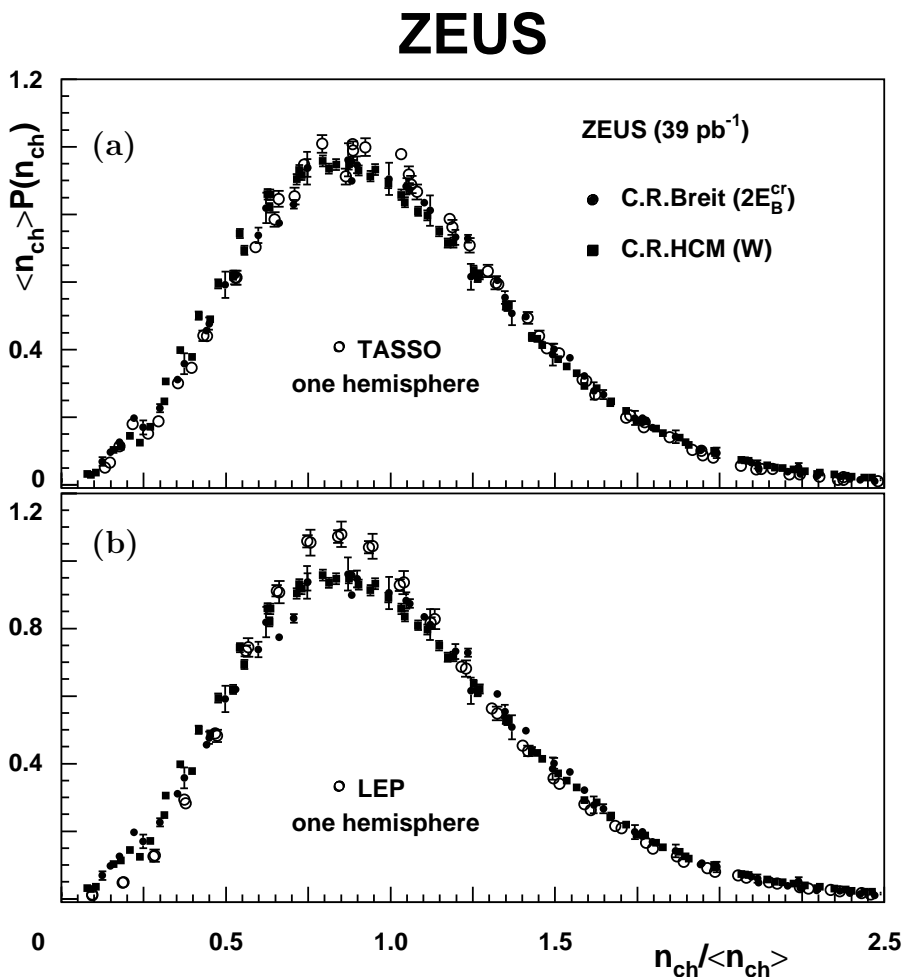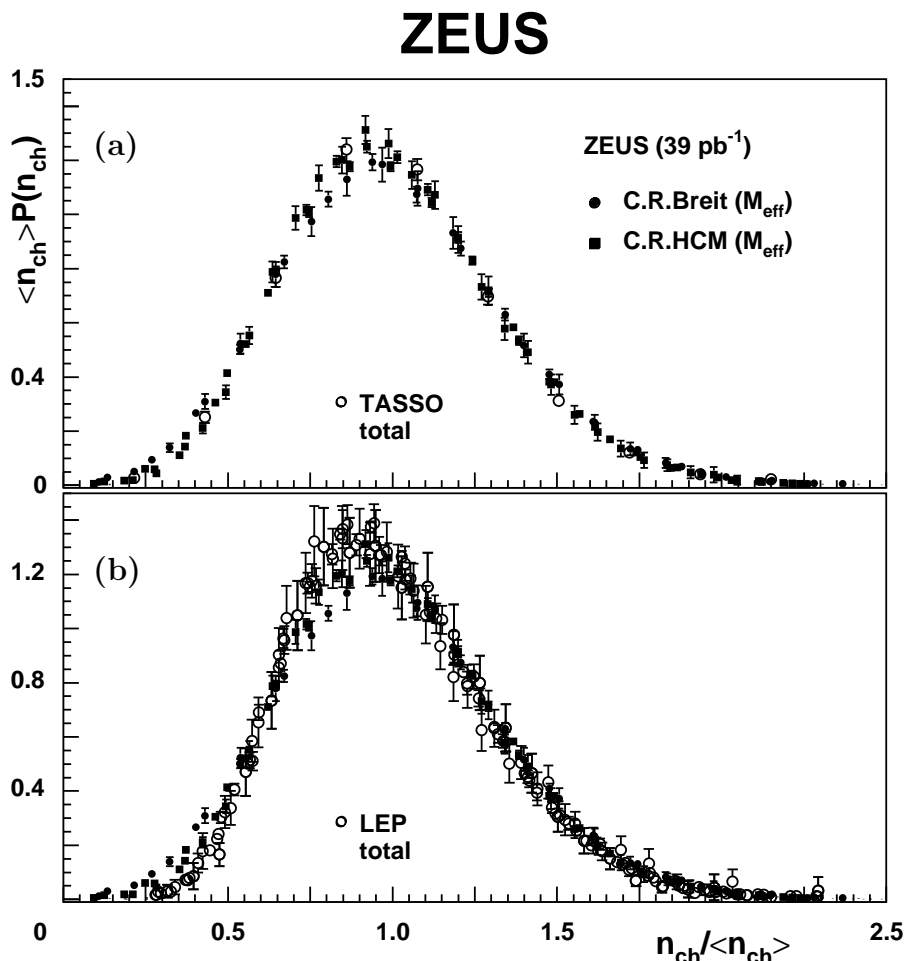
ZEUS

Figure 7: The multiplicity distributions plotted in KNO form and compared to the results of e^+e^- experiments. The solid circles represent the ZEUS data measured in the current region of the Breit frame in bins of $2 \cdot E_\mathrm{B}^\mathrm{cr}$, for $2 \cdot E_\mathrm{B}^\mathrm{cr} \geq 12$ GeV, and the solid squares represent the data measured in the current region of the HCM frame in bins of W. Multiplicities measured in one hemisphere of the e^+e^- collision are shown in bins of $\sqrt{s_\mathrm{ee}}$ for (a) the TASSO experiment [41], in the energy range $14 \leq \sqrt{s_\mathrm{ee}} \leq 44$ GeV, and (b) for the LEP experiments [42, 43], measured at energy $\sqrt{s_\mathrm{ee}} = 91.2$ GeV.

hadronic system, M_eff. In figures 10(a) and 10(b), the multiplicities are compared to the MC predictions. All three MC models describe the data reasonably well; however in the last M_eff bin in the current region of the HCM, the HERWIG prediction is too high. In figure 10(c), both measurements are shown together and compared with different MC curves calculated using the ARIADNE MC. The measurements in the Breit and HCM frames agree at values of M_eff less than 10 GeV. Above this value, $\langle n_\mathrm{ch} \rangle$ rises much faster with M_eff in the current region of the HCM frame than in the current region of the Breit frame. Since the HCM measurement was restricted in η, a separate ARIADNE calculation was performed in the total current region of the HCM frame. The difference is small, although the rise of

Figure 8: The multiplicity distributions plotted in KNO form and compared to the results of the e^+e^- experiments. The solid circles represent the ZEUS data measured in the current region of the Breit frame and the solid squares represent the data measured in the current region of the HCM frame both in bins of M_{eff}, for $M_{\text{eff}} \geq 8$ GeV. Charged multiplicities measured for the whole event in e^+e^- collisions are shown in bins of $\sqrt{s_{\text{ee}}}$ for (a) the TASSO experiment [41], in the energy range $14 \leq \sqrt{s_{\text{ee}}} \leq 44$ GeV, and (b) for the LEP experiments [42–56] in the energy range $91.2 \leq \sqrt{s_{\text{ee}}} \leq 209$ GeV.

$\langle n_{\text{ch}} \rangle$ with M_{eff} is faster in the total current region of the HCM frame.

Figure 10(c) also shows $2 \cdot \langle n_{\text{ch}} \rangle$ as a function of $2 \cdot E_{\text{B}}^{\text{cr}}$. This measurement exhibits the same behaviour as $\langle n_{\text{ch}} \rangle$ as a function of M_{eff} in the current region of the Breit frame but differs from that in the HCM frame. The multiplicity in the current region of the HCM frame rises much faster with the invariant mass than with W.

Finally, figure 11 combines the mean charged multiplicities measured in the current regions of the Breit and HCM frames as functions of the respective energy scales, $2 \cdot E_{\text{B}}^{\text{cr}}$ and W. Also shown are the measurements from e^+e^- [41–59] and fixed-target [8–10] experiments. The fixed-target data were scaled by a factor two, since they only measure one hemisphere and by a factor 1.08, to correct for the decays of the K_S^0 and Λ, as estimated using ARIADNE MC.
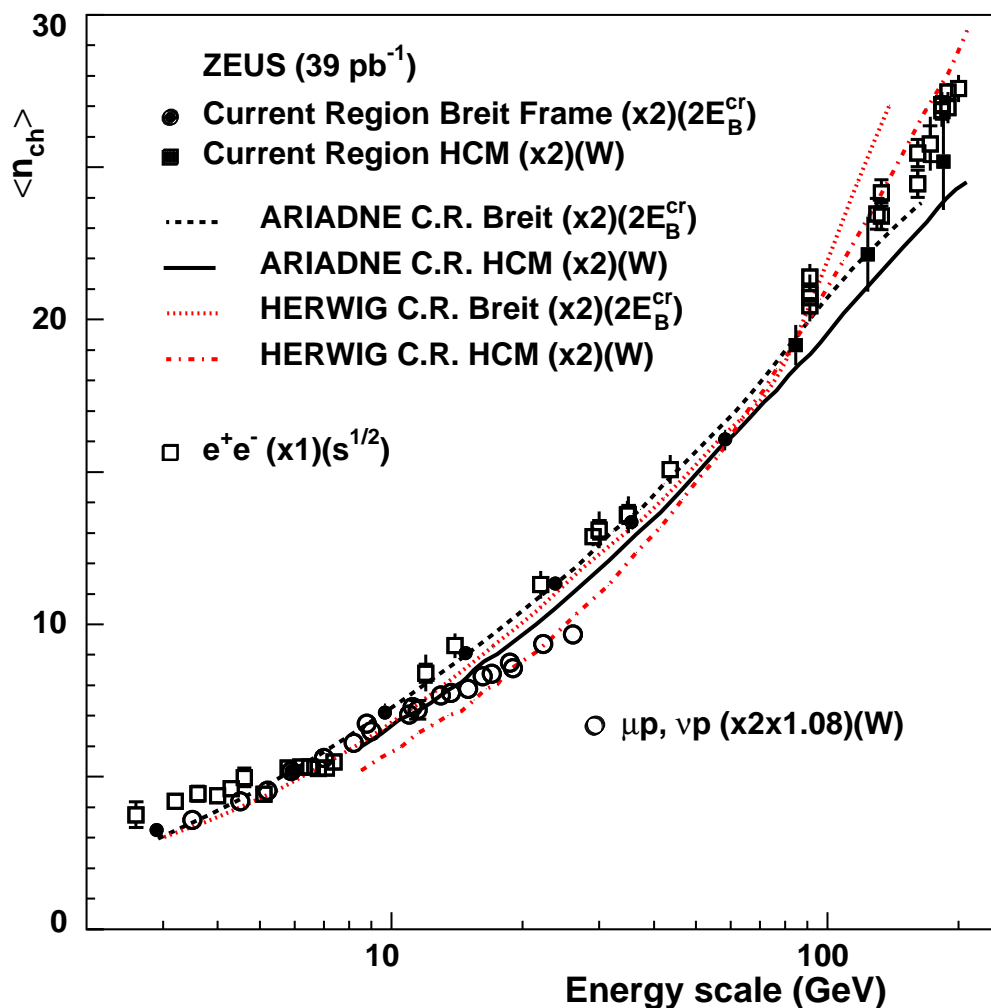
ZEUS
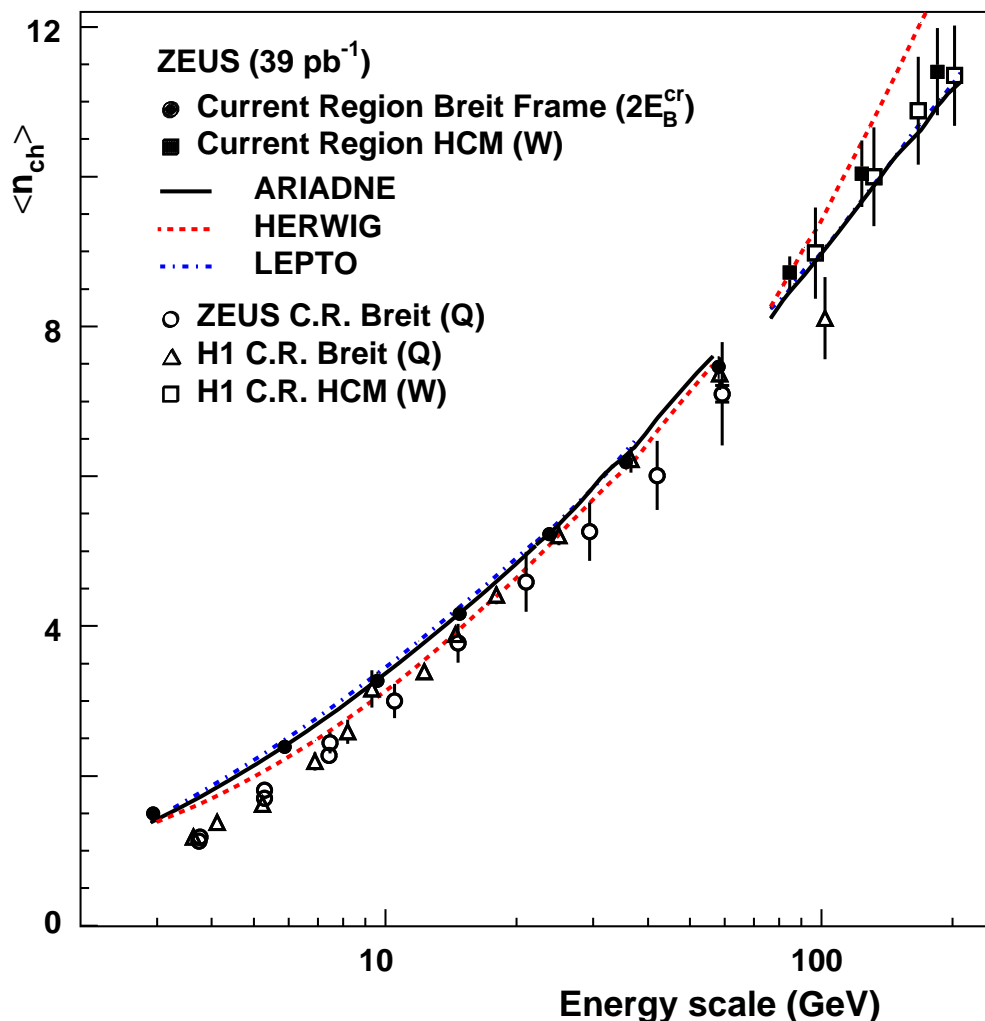
Figure 9: Mean charged multiplicity, $\langle n_{\mathrm{ch}} \rangle$, in the current region of the Breit frame as a function of $2 \cdot E_{\mathrm{B}}^{\mathrm{cr}}$ and in the current fragmentation region of the HCM frame as a function of W. The inner error bars represent the statistical uncertainties, typically smaller than the size of the symbols. The outer error bars represent the quadratic sum of statistical and systematic uncertainties. Also shown are the results of previous HERA measurements [1, 2, 4, 5] and predictions from ARIADNE, LEPTO and HERWIG. The decay products of K_S^0 and Λ are not included.

The measurements presented in this paper show good overall agreement with those from other experiments, exhibiting approximately the same dependence of the mean charged multiplicity on the respective energy scale. At low values of the energy, the measurement as a function of $2 \cdot E_{\mathrm{B}}^{\mathrm{cr}}$ agrees well with $e^+ e^-$ data, in contrast to the previous measurements as a function of Q [2, 5]. The measurements in the current region of the HCM agree with the LEP data, but are systematically below them. The data from fixed-

ZEUS
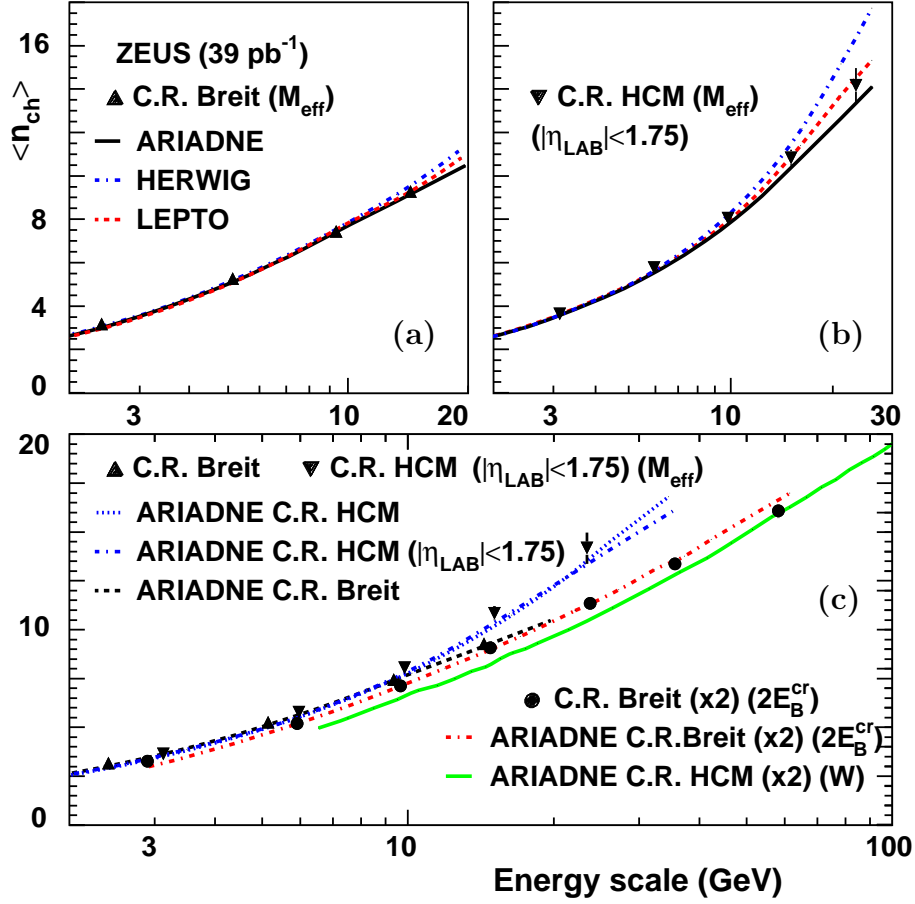
Figure 10: Mean charged multiplicity, $\langle n_{ch} \rangle$, measured as a function of M_{eff} (a) in the current region of the Breit frame and (b) in the current region of the HCM frame compared to MC predictions. (c) Comparison between measurements in the current regions of the Breit and HCM frame as functions of M_{eff} and with the measurement as a function of $2 \cdot E_B^{cr}$. The predictions from ARIADNE are also shown.

target DIS experiments [1, 8 – 10] deviate from the observed energy dependence at energies above 15 GeV. The ARIADNE MC prediction generally describes the energy dependence of the data over the entire region. However, the prediction in the HCM frame is generally lower than the data and than the prediction in the Breit frame. The HERWIG MC model does not give a good overall description of the data.

7. Summary and conclusions

The charged multiplicity distributions and the mean charged multiplicity have been investigated in inclusive neutral current deep inelastic ep scattering in the kinematic range $Q^2 > 25 \, \text{GeV}^2$ and $70 < W < 225 \, \text{GeV}$ in terms of different energy scales. The scale $2 \cdot E_B^{cr}$,

Figure 11: Mean charged multiplicity, $\langle n_{\rm ch} \rangle$, in the current region of the Breit frame multiplied by 2 as a function of $2 \cdot E_{\rm B}^{\rm cr}$ and in the current region of the HCM frame multiplied by 2 as a function of W. The results of e^+e^- [41–59] and fixed-target DIS experiments [8–10] are shown. The factor 1.08 was estimated using MC predictions to correct the fixed-target data for the decay products of K_S^0 and Λ. The predictions of ARIADNE and HERWIG are also shown.

was used in the current region of the Breit frame. In the current region of the HCM frame, W was used and the invariant mass, $M_{\rm eff}$, was used in both frames.

In terms of KNO scaling, the charged multiplicities in the current regions of the Breit and HCM frames exhibit the same behaviour as those in one hemisphere of e^+e^- collisions when $2 \cdot E_{\rm B}^{\rm cr}$ or W are considered. When the energy scale $M_{\rm eff}$ is used, the charged multiplicities exhibit the same KNO-scaling behaviour as those for the whole e^+e^- event.

The mean charged multiplicity in the current region of the Breit frame scales with $M_{\rm eff}$

Current region of the Breit frame		
$M_{\rm eff}$ (GeV)	$\langle n_{\rm ch} \rangle$ (K^0, Λ stable)	$\langle n_{\rm ch} \rangle$ (K^0, Λ decay)
2.4	$2.91 \pm 0.01^{+0.04}_{-0.03}$	$3.17 \pm 0.01^{+0.04}_{-0.03}$
5.2	$4.82 \pm 0.02^{+0.03}_{-0.03}$	$5.26 \pm 0.02^{+0.03}_{-0.03}$
9.4	$6.85 \pm 0.02^{+0.07}_{-0.05}$	$7.45 \pm 0.02^{+0.08}_{-0.06}$
14.4	$8.60 \pm 0.06^{+0.07}_{-0.09}$	$9.29 \pm 0.06^{+0.14}_{-0.09}$
Current region of the HCM frame		
$M_{\rm eff}$ (GeV)	$\langle n_{\rm ch} \rangle$ (K^0, Λ stable)	$\langle n_{\rm ch} \rangle$ (K^0, Λ decay)
3.1	$3.38 \pm 0.02^{+0.03}_{-0.02}$	$3.64 \pm 0.02^{+0.05}_{-0.02}$
5.9	$5.33 \pm 0.01^{+0.07}_{-0.07}$	$5.77 \pm 0.01^{+0.09}_{-0.09}$
9.8	$7.37 \pm 0.02^{+0.13}_{-0.12}$	$8.05 \pm 0.01^{+0.19}_{-0.19}$
15.1	$9.86 \pm 0.02^{+0.23}_{-0.23}$	$10.84 \pm 0.02^{+0.36}_{-0.36}$
23.5	$12.83 \pm 0.06^{+0.53}_{-0.54}$	$14.17 \pm 0.05^{+0.80}_{-0.80}$

Table 6: Mean charged multiplicity, $\langle n_{\rm ch} \rangle$, measured in the current region of the Breit frame and in the current fragmentation region of the HCM frame as a function of $M_{\rm eff}$. The first errors are statistical and the second are the systematic uncertainties.

in the same way as $2 \cdot \langle n_{\rm ch} \rangle$ scales with $2 \cdot E_{\rm B}^{\rm cr}$ and, therefore, as $\langle n_{\rm ch} \rangle$ scales with $\sqrt{s_{\rm ee}}$ in e^+e^- collisions. The mean charged multiplicity in the current region of HCM frame as a function of $M_{\rm eff}$ rises faster than that in the current region of the Breit frame.

The energy scale $2 \cdot E_{\rm B}^{\rm cr}$, rather than Q, gives better agreement between the mean charged multiplicity measured in the current region of the Breit frame and that measured in e^+e^- collisions. The measurements of $\langle n_{\rm ch} \rangle$ as a function of W agree, within the uncertainties, with the data from e^+e^- collisions. When using these scales, ep DIS data can be consistently compared with data from e^+e^-, μP and νP scattering over a wide energy region.

Acknowledgments

Author list

S. Chekanov, M. Derrick, S. Magill, B. Musgrave, D. Nicholass,[1] J. Repond and R. Yoshida
Argonne National Laboratory,
Argonne, Illinois 60439-4815, U.S.A.[n]

M.C.K. Mattingly
Andrews University,
Berrien Springs, Michigan 49104-0380, U.S.A.

M. Jechow and N. Pavel[†]
Institut für Physik der Humboldt-Universität zu Berlin,
Berlin, Germany[b]

P. Antonioli, G. Bari, L. Bellagamba, D. Boscherini, A. Bruni, G. Bruni, F. Cindolo, M. Corradi, G. Iacobucci, A. Margotti, R. Nania and A. Polini
INFN Bologna,
Bologna, Italy[e]

S. Antonelli, M. Basile, M. Bindi, L. Cifarelli, A. Contin, S. De Pasquale,[2] G. Sartorelli and A. Zichichi
University and INFN Bologna,
Bologna, Italy[e]

D. Bartsch, I. Brock, H. Hartmann, E. Hilger, H.-P. Jakob, M. Jüngst, A.E. Nuncio-Quiroz, E. Paul,[3] U. Samson, V. Schönberg, R. Shehzadi and M. Wlasenko
Physikalisches Institut der Universität Bonn,
Bonn, Germany[b]

N.H. Brook, G.P. Heath, J.D. Morris and A. Solomin
H.H. Wills Physics Laboratory, University of Bristol,
Bristol, U.K.[m]

M. Capua, S. Fazio, A. Mastroberardino, M. Schioppa, G. Susinno and E. Tassi
Calabria University, Physics Department and INFN,
Cosenza, Italy[e]

J.Y. Kim
Chonnam National University,
Kwangju, South Korea

Z.A. Ibrahim, B. Kamaluddin and W.A.T. Wan Abdullah
Jabatan Fizik, Universiti Malaya,
50603 Kuala Lumpur, Malaysia[r]

Y. Ning, Z. Ren and F. Sciulli
Nevis Laboratories, Columbia University,
Irvington on Hudson, New York 10027, U.S.A.[o]

J. Chwastowski, A. Eskreys, J. Figiel, A. Galas, M. Gil, K. Olkiewicz, P. Stopa and L. Zawiejski
The Henryk Niewodniczanski Institute of Nuclear Physics, Polish Academy of Sciences,
Cracow, Poland[i]

L. Adamczyk, T. Bołd, I. Grabowska-Bołd, D. Kisielewska, J. Łukasik, M. Przybycień and L. Suszycki
Faculty of Physics and Applied Computer Science, AGH-University of Science and Technology,
Cracow, Poland[p]

A. Kotański[4] and W. Słomiński[5]
Department of Physics, Jagellonian University,
Cracow, Poland

U. Behrens, C. Blohm, A. Bonato, K. Borras, R. Ciesielski, N. Coppola, S. Fang, J. Fourletova,[6] A. Geiser, P. Göttlicher,[7] J. Grebenyuk, I. Gregor, T. Haas, W. Hain, A. Hüttmann, F. Januschek, B. Kahle, I.I. Katkov, U. Klein,[8] U. Kötz,[3] H. Kowalski, E. Lobodzinska, B. Löhr,[3] R. Mankel, I.-A. Melzer-Pellmann, S. Miglioranzi, A. Montanari, T. Namsoo, D. Notz,[9] A. Parenti, L. Rinaldi,[10] P. Roloff, I. Rubinsky, R. Santamarta,[11] U. Schneekloth, A. Spiridonov,[12] D. Szuba,[13] J. Szuba,[14] T. Theedt, G. Wolf,[3] K. Wrona, A.G. Yagües Molina, C. Youngman and W. Zeuner[9]
Deutsches Elektronen-Synchrotron DESY,
Hamburg, Germany

V. Drugakov, W. Lohmann and S. Schlenstedt
Deutsches Elektronen-Synchrotron DESY,
Zeuthen, Germany

G. Barbagli and E. Gallo
INFN Florence,
Florence, Italy[e]

P. G. Pelfer

University and INFN Florence,
Florence, Italy[e]

A. Bamberger, D. Dobur, F. Karstens and N.N. Vlasov[15]

Fakultät für Physik der Universität Freiburg i.Br.,
Freiburg i.Br., Germany[b]

P.J. Bussey,[16] A.T. Doyle, W. Dunne, M. Forrest, M. Rosin, D.H. Saxon and I.O. Skillicorn

Department of Physics and Astronomy, University of Glasgow,
Glasgow, U.K.[m]

I. Gialas[17] and K. Papageorgiu

Department of Engineering in Management and Finance, Univ. of Aegean,
Greece

U. Holm, R. Klanner, E. Lohrmann, P. Schleper, T. Schörner-Sadenius, J. Sztuk, H. Stadie and M. Turcato

Hamburg University, Institute of Exp. Physics,
Hamburg, Germany[b]

C. Foudas, C. Fry, K.R. Long and A.D. Tapper

Imperial College London, High Energy Nuclear Physics Group,
London, U.K.[m]

T. Matsumoto, K. Nagano, K. Tokushuku,[18] S. Yamada and Y. Yamazaki[19]

Institute of Particle and Nuclear Studies, KEK,
Tsukuba, Japan[f]

A.N. Barakbaev, E.G. Boos,[3] N.S. Pokrovskiy and B.O. Zhautykov

Institute of Physics and Technology of Ministry of Education and Science of Kazakhstan,
Almaty, Kazakhstan

V. Aushev,[20] M. Borodin, I. Kadenko, A. Kozulia, V. Libov, M. Lisovyi, D. Lontkovskyi, I. Makarenko, Iu. Sorokin, A. Verbytskyi and O. Volynets

Institute for Nuclear Research, National Academy of Sciences, Kiev, Ukraine, and
Kiev National University,
Kiev, Ukraine

D. Son

Kyungpook National University, Center for High Energy Physics,
Daegu, South Korea[g]

J. de Favereau and K. Piotrzkowski
Institut de Physique Nucléaire, Université Catholique de Louvain,
Louvain-la-Neuve, Belgium[q]

F. Barreiro, C. Glasman, M. Jimenez, L. Labarga, J. del Peso, E. Ron,
M. Soares, J. Terrón and M. Zambrana
Departamento de Física Teórica, Universidad Autónoma de Madrid,
Madrid, Spain[l]

F. Corriveau, C. Liu, J. Schwartz, R. Walsh and C. Zhou
Department of Physics, McGill University,
Montréal, Québec, H3A 2T8 Canada[a]

T. Tsurugai
Meiji Gakuin University, Faculty of General Education,
Yokohama, Japan[f]

A. Antonov, B.A. Dolgoshein, D. Gladkov, V. Sosnovtsev, A. Stifutkin
and S. Suchkov
Moscow Engineering Physics Institute,
Moscow, Russia[j]

R.K. Dementiev, P.F. Ermolov, L.K. Gladilin, Yu.A. Golubkov, L.A. Khein,
I.A. Korzhavina, V.A. Kuzmin, B.B. Levchenko,[21] O.Yu. Lukina,
A.S. Proskuryakov, L.M. Shcheglova and D.S. Zotkin
Moscow State University, Institute of Nuclear Physics,
Moscow, Russia[k]

I. Abt, A. Caldwell, D. Kollar, B. Reisert and W.B. Schmidke
Max-Planck-Institut für Physik,
München, Germany

G. Grigorescu, A. Keramidas, E. Koffeman, P. Kooijman, A. Pellegrino,
H. Tiecke, M. Vázquez[9] and L. Wiggers
NIKHEF and University of Amsterdam,
Amsterdam, Netherlands[h]

N. Brümmer, B. Bylsma, L.S. Durkin, A. Lee and T.Y. Ling
Physics Department, Ohio State University,
Columbus, Ohio 43210, U.S.A.[n]

P.D. Allfrey, M.A. Bell, A.M. Cooper-Sarkar, R.C.E. Devenish, J. Ferrando, B. Foster, K. Korcsak-Gorzo, K. Oliver, S. Patel, V. Roberfroid,[22] A. Robertson, P.B. Straub, C. Uribe-Estrada and R. Walczak

Department of Physics, University of Oxford,
Oxford, U.K.[m]

A. Bertolin, F. Dal Corso, S. Dusini, A. Longhin and L. Stanco

INFN Padova,
Padova, Italy[e]

P. Bellan, R. Brugnera, R. Carlin, A. Garfagnini and S. Limentani

Dipartimento di Fisica dell' Università and INFN,
Padova, Italy[e]

B.Y. Oh, A. Raval, J. Ukleja[23] and J.J. Whitmore[24]

Department of Physics, Pennsylvania State University,
University Park, Pennsylvania 16802, U.S.A.[o]

Y. Iga

Polytechnic University,
Sagamihara, Japan[f]

G. D'Agostini, G. Marini and A. Nigro

Dipartimento di Fisica, Università 'La Sapienza' and INFN,
Rome, Italy[e]

J.E. Cole and J.C. Hart

Rutherford Appleton Laboratory,
Chilton, Didcot, Oxon, U.K.[m]

H. Abramowicz,[25] R. Ingbir, S. Kananov, A. Levy and A. Stern

Raymond and Beverly Sackler Faculty of Exact Sciences,
School of Physics, Tel-Aviv University,
Tel-Aviv, Israel[d]

M. Kuze and J. Maeda

Department of Physics, Tokyo Institute of Technology,
Tokyo, Japan[f]

R. Hori, S. Kagawa,[26] N. Okazaki, S. Shimizu and T. Tawara

Department of Physics, University of Tokyo,
Tokyo, Japan[f]

R. Hamatsu, H. Kaji,[27] **S. Kitamura,**[28] **O. Ota and Y.D. Ri**

Department of Physics, Tokyo Metropolitan University,
Tokyo, Japan[f]

M. Costa, M.I. Ferrero, V. Monaco, R. Sacchi and A. Solano

Università di Torino and INFN,
Torino, Italy[e]

M. Arneodo and M. Ruspa

Università del Piemonte Orientale,
Novara Italy, and
INFN,
Torino, Italy[e]

S. Fourletov,[6] **J.F. Martin and T.P. Stewart**

Department of Physics, University of Toronto,
Toronto, Ontario, M5S 1A7 Canada[a]

S.K. Boutle,[17] **J.M. Butterworth, C. Gwenlan,**[29] **T.W. Jones, J.H. Loizides**
and M. Wing[30]

Physics and Astronomy Department, University College London,
London, U.K.[m]

B. Brzozowska, J. Ciborowski,[31] **G. Grzelak, P. Kulinski, P. Łużniak,**[32]
J. Malka,[32] **R.J. Nowak, J.M. Pawlak, T. Tymieniecka, A. Ukleja and**
A.F. Żarnecki

Warsaw University, Institute of Experimental Physics,
Warsaw, Poland

M. Adamus and P. Plucinski[33]

Institute for Nuclear Studies,
Warsaw, Poland

Y. Eisenberg, D. Hochman and U. Karshon

Department of Particle Physics, Weizmann Institute,
Rehovot, Israel[c]

E. Brownson, T. Danielson, A. Everett, D. Kçira, D.D. Reeder,[3] **P. Ryan,**
A.A. Savin, W.H. Smith and H. Wolfe

Department of Physics, University of Wisconsin,
Madison, Wisconsin 53706, U.S.A.[n]

S. Bhadra, C.D. Catterall, Y. Cui, G. Hartner, S. Menary, U. Noor, J. Standage and J. Whyte

Department of Physics, York University,
Ontario, M3J 1P3 Canada[a]

References

[1] H1 collaboration, S. Aid et al., *Charged particle multiplicities in deep inelastic scattering at HERA*, *Z. Physik* **C 72** (1996) 573 [`hep-ex/9608011`].

[2] H1 collaboration, C. Adloff et al., *Evolution of ep fragmentation and multiplicity distributions in the Breit frame*, *Nucl. Phys.* **B 504** (1997) 3 [`hep-ex/9707005`].

[3] H1 collaboration, C. Adloff et al., *Multiplicity structure of the hadronic final state in diffractive deep-inelastic scattering at HERA*, *Eur. Phys. J.* **C 5** (1998) 439 [`hep-ex/9804012`].

[4] H1 collaboration, F.D. Aaron et al., *Charged particle production in high Q2 deep-inelastic scattering at HERA*, *Phys. Lett.* **B 654** (2007) 148 [arXiv:0706.2456].

[5] ZEUS collaboration, M. Derrick et al., *Measurement of multiplicity and momentum spectra in the current fragmentation region of the Breit frame at HERA*, *Z. Physik* **C 67** (1995) 93 [hep-ex/9501012].

[6] ZEUS collaboration, J. Breitweg et al., *Measurement of multiplicity and momentum spectra in the current and target regions of the Breit frame in deep inelastic scattering at HERA*, *Eur. Phys. J.* **C 11** (1999) 251 [hep-ex/9903056].

[7] ZEUS collaboration, S. Chekanov et al., *Multiplicity moments in deep inelastic scattering at HERA*, *Phys. Lett.* **B 510** (2001) 36 [hep-ex/0104036].

[8] E665 collaboration, M.R. Adams et al., *Inclusive single-particle distributions and transverse momenta of forward produced charged hadrons in μ p scattering at 470 GeV*, *Z. Physik* **C 76** (1997) 441.

[9] EUROPEAN MUON collaboration, M. Arneodo et al., *Comparison of multiplicity distributions to the negative binomial distribution in muon-proton scattering*, *Z. Physik* **C 35** (1987) 335 [*Erratum ibid.* **C 36** (1987) 512].

[10] G.T. Jones et al., *Multiplicity distributions of charged hadrons in neutrino p and anti-neutrino p charged current interactions*, *Z. Physik* **C 54** (1992) 45.

[11] NOMAD collaboration, J. Altegoer et al., *Precision measurement of scaled momentum, charge multiplicity and thrust in ν_μ N and $\bar{\nu}_\mu$ N interactions*, *Phys. Lett.* **B 445** (1999) 439.

[12] ZEUS collaboration, U. Holm ed., *The ZEUS detector*, status report unpublished, http://www-zeus.desy.de/bluebook/bluebook.html, DESY, Germany (1993)

[13] N. Harnew et al., *Vertex triggering using time difference measurements in the ZEUS central tracking detector*, *Nucl. Instrum. Meth.* **A279** (1989) 290.

[14] B. Foster et al., *The performance of the ZEUS central tracking detector z-by-timing electronics in a transputer based data acquisition system*, *Nucl. Phys.* **32** (Proc. Suppl.) (1993) 181.

[15] ZEUS collaboration, B. Foster et al., *The design and construction of the ZEUS central tracking detector*, *Nucl. Instrum. Meth.* **A338** (1994) 254.

[16] M. Derrick et al., *Design and construction of the ZEUS barrel calorimeter*, *Nucl. Instrum. Meth.* **A309** (1991) 77.

[17] ZEUS CALORIMETER GROUP and ZEUS collaboration, A. Andresen et al., *Construction and beam test of the ZEUS forward and rear calorimeter*, *Nucl. Instrum. Meth.* **A309** (1991) 101.

[18] A. Caldwell et al., *Design and implementation of a high precision readout system for the ZEUS calorimeter*, *Nucl. Instrum. Meth.* **A321** (1992) 356.

[19] ZEUS BARREL CALORIMETER GROUP collaboration, A. Bernstein et al., *Beam tests of the ZEUS barrel calorimeter*, *Nucl. Instrum. Meth.* **A336** (1993) 23.

[20] H. Abramowicz, A. Caldwell and R. Sinkus, *Neural network based electron identification in the ZEUS calorimeter*, *Nucl. Instrum. Meth.* **A365** (1995) 508 [hep-ex/9505004].

[21] S. Bentvelsen, J. Engelen and P. Kooijman, *Reconstruction of (x, Q^2) and extraction of structure functions in neutral current scattering at HERA*, NIKHEF-H-92-02.

[22] G.M. Briskin, *Diffractive dissociation in ep deep inelastic scattering*, DESY-THESIS-1998-036.

[23] J.E. Huth et al., *Toward a standardization of jet definitions*, FERMILAB-CONF-90-249-E.

[24] F. Jacquet and A. Blondel, in U. Amaldi ed., *Proceedings of the study of an eP facility for Europe*, DESY-79-48.

[25] K.H. Streng, T.F. Walsh and P.M. Zerwas, *Quark and gluon jets in the Breit frame of lepton-nucleon scattering*, *Z. Physik* **C 2** (1979) 237.

[26] L. Lönnblad, *ARIADNE version 4: a program for simulation of QCD cascades implementing the color dipole model*, *Comput. Phys. Commun.* **71** (1992) 15.

[27] G. Ingelman, A. Edin and J. Rathsman, *LEPTO* 6.5*: a Monte Carlo generator for deep inelastic lepton-nucleon scattering*, *Comput. Phys. Commun.* **101** (1997) 108 [hep-ph/9605286].

[28] A. Kwiatkowski, H. Spiesberger and H.-J. Möhring, *Heracles: an event generator for ep interactions at HERA energies including radiative processes: version 1.0*, *Comput. Phys. Commun.* **69** (1992) 155.

[29] H. Spiesberger, *An event generator for ep interactions at HERA including radiative processes (version 4.6)*, 1996, available on http://www.desy.de/~hspiesb/heracles.html.

[30] H. Spiesberger, HERACLES *and* DJANGOH*: event generation for ep interactions at HERA including radiative processes*, available on http://wwwthep.physik.uni-mainz.de/~hspiesb/djangoh/djangoh.html (1998).

[31] K. Charchula, G.A. Schuler and H. Spiesberger, *Combined QED and QCD radiative effects in deep inelastic lepton-proton scattering: the Monte Carlo generator DJANGO6*, *Comput. Phys. Commun.* **81** (1994) 381.

[32] B. Andersson, G. Gustafson, G. Ingelman and T. Sjöstrand, *Parton fragmentation and string dynamics*, *Phys. Rept.* **97** (1983) 31.

[33] H.L. Lai et al., *Improved parton distributions from global analysis of recent deep inelastic scattering and inclusive jet data*, *Phys. Rev.* **D 55** (1997) 1280 [hep-ph/9606399].

[34] G. Marchesini et al., *HERWIG: a Monte Carlo event generator for simulating hadron emission reactions with interfering gluons. Version 5.1 — april 1991*, *Comput. Phys. Commun.* **67** (1992) 465.

[35] ZEUS collaboration, S. Chekanov et al., *Photoproduction of events with rapidity gaps between jets at HERA*, *Eur. Phys. J.* **C 50** (2007) 283 [hep-ex/0612008].

[36] CTEQ collaboration, H.L. Lai et al., *Global QCD analysis of parton structure of the nucleon: cTEQ5 parton distributions*, *Eur. Phys. J.* **C 12** (2000) 375 [hep-ph/9903282].

[37] R. Brun et al. ed., GEANT3, CERN-DD/EE/84-1.

[38] M.L. Rosin, *Energy dependence of the mean charged multiplicity in deep inelastic scattering with ZEUS at HERA*, UMI-32-22954.

[39] M. Gazdzicki, R. Szwed, G. Wrochna and A.K. Wroblewski, *Scaling of multiplicity distributions and collision dynamics in e^+e^- and pp interactions*, *Mod. Phys. Lett.* **A 6** (1991) 981.

[40] Z. Koba, H.B. Nielsen and P. Olesen, *Scaling of multiplicity distributions in high-energy hadron collisions*, *Nucl. Phys.* **B 40** (1972) 317.

[41] TASSO collaboration, W. Braunschweig et al., *Charged multiplicity distributions and correlations in e^+e^- annihilation at PETRA energies*, *Z. Physik* **C 45** (1989) 193.

[42] DELPHI collaboration, P. Abreu et al., *Charged particle multiplicity distributions in Z0 hadronic decays*, *Z. Physik* **C 50** (1991) 185.

[43] OPAL collaboration, P.D. Acton et al., *A study of charged particle multiplicities in hadronic decays of the Z0*, *Z. Physik* **C 53** (1992) 539.

[44] ALEPH collaboration, D. Decamp et al., *Measurement of the charged particle multiplicity distribution in hadronic Z decays*, *Phys. Lett.* **B 273** (1991) 181.

[45] ALEPH collaboration, D. Buskulic et al., *Studies of QCD in $e^+e^- \to$ hadrons at $E_{cm} = 130\,GeV$ and $136\,GeV$*, *Z. Physik* **C 73** (1997) 409.

[46] DELPHI collaboration, P. Abreu et al., *Charged particle multiplicity in e^+e^- interactions at $\sqrt{s} = 130\,GeV$*, *Phys. Lett.* **B 372** (1996) 172.

[47] DELPHI collaboration, P. Abreu et al., *Charged particle multiplicity in $e^+e^- \to q\bar{q}$ events at $161\,GeV$ and $172\,GeV$ and from the decay of the W boson*, *Phys. Lett.* **B 416** (1998) 233.

[48] DELPHI collaboration, P. Abreu et al., *Charged and identified particles in the hadronic decay of W bosons and in $e^+e^- \to q\bar{q}$ from 130 to $200\,GeV$*, *Eur. Phys. J.* **C 18** (2000) 203 [*Erratum ibid.* **C 25** (2002) 493] [`hep-ex/0103031`].

[49] L3 collaboration, P. Achard et al., *Studies of hadronic event structure in e^+e^- annihilation from $30\,GeV$ to $209\,GeV$ with the L3 detector*, *Phys. Rept.* **399** (2004) 71 [`hep-ex/0406049`].

[50] L3 collaboration, P. Achard et al., *Measurement of charged-particle multiplicity distributions and their H_q moments in hadronic Z decays at LEP*, *Phys. Lett.* **B 577** (2003) 109 [`hep-ex/0110072`].

[51] L3 collaboration, M. Acciarri et al., *Study of the structure of hadronic events and determination of alpha-s at $\sqrt{s} = 130\,GeV$ and $136\,GeV$*, *Phys. Lett.* **B 371** (1996) 137.

[52] L3 collaboration, M. Acciarri et al., *QCD studies and determination of α_s in e^+e^- collisions at $\sqrt{s} = 161\,GeV$ and $172\,GeV$*, *Phys. Lett.* **B 404** (1997) 390.

[53] L3 collaboration, M. Acciarri et al., *QCD results from studies of hadronic events produced in e^+e^- annihilations at $\sqrt{s} = 183\,GeV$*, *Phys. Lett.* **B 444** (1998) 569.

[54] OPAL collaboration, G. Alexander et al., *QCD studies with e^+e^- annihilation data at $130\,GeV$ and $136\,GeV$*, *Z. Physik* **C 72** (1996) 191.

[55] OPAL collaboration, K. Ackerstaff et al., *QCD studies with e^+e^- annihilation data at $161\,GeV$*, *Z. Physik* **C 75** (1997) 193.

[56] OPAL collaboration, G. Abbiendi et al., *QCD studies with e^+e^- annihilation data at $172\,GeV$ to $189\,GeV$*, *Eur. Phys. J.* **C 16** (2000) 185 [`hep-ex/0002012`].

[57] MARK I collaboration, V. Luth et al., *K0 production in e^+e^- annihilation*, *Phys. Lett.* **B 70** (1977) 120.

[58] JADE collaboration, W. Bartel et al., *Charged particle and neutral kaon production in e^+e^- annihilation at PETRA*, *Z. Physik* **C 20** (1983) 187.

[59] M. Derrick et al., *Study of quark fragmentation in e^+e^- annihilation at $29\,GeV$: charged particle multiplicity and single particle rapidity distributions*, *Phys. Rev.* **D 34** (1986) 3304.